Plasma Instrument Design: Outline

Dr. James McFadden, UC Berkeley

Outline:

- **Particle detectors**
- **Analog Signal Processing**
- **Analyzers**
- **How to Design an instrument**
- **Calibration Issues**
- **Example Instruments**

Plasma Instrument Design: Examples

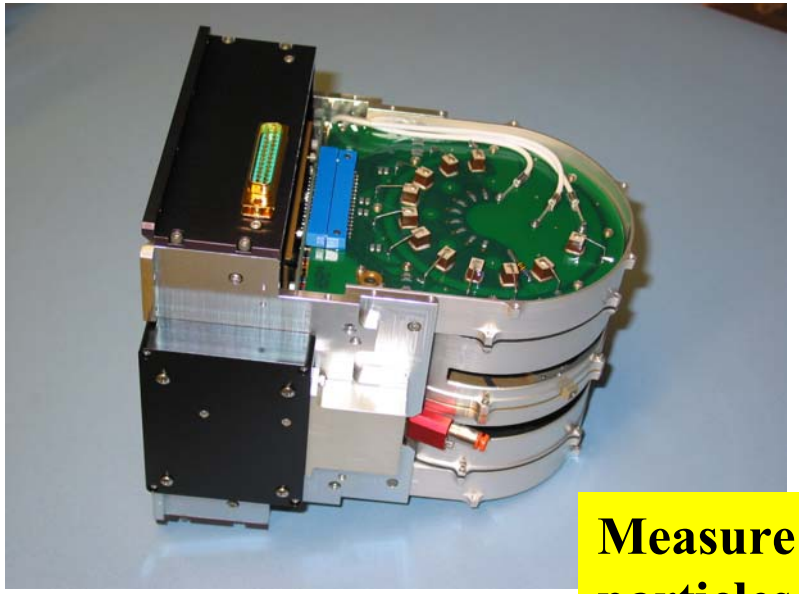

Measure charged particles from ~1 eV to ~30 keV

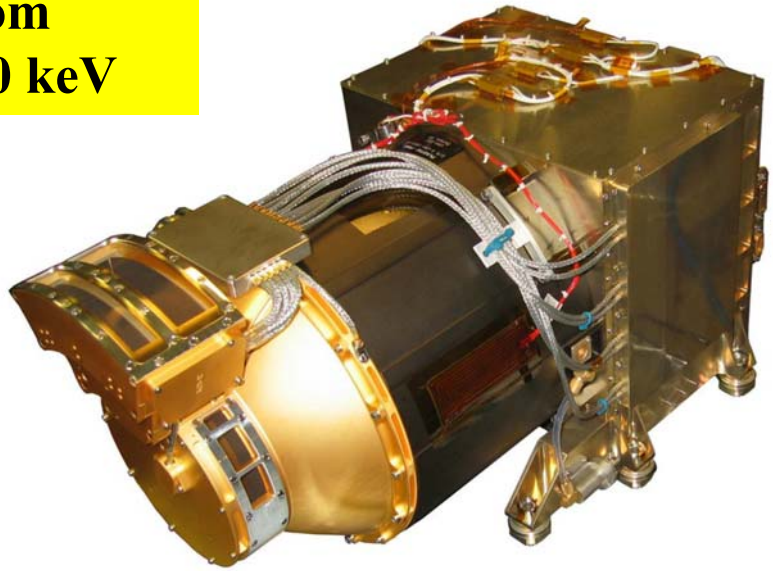

Plasma Instrument Design: Outline

Some Types of Instrument Design:

Developing a new technology (rare)

Recognizing a use for new technology

(paying attention at the right place, right time)

Miniaturize a known technology (expensive)

New optics for known technology (clever)

Combining known technologies (innovative)

Improve features of a technology (perfectionist)

Simplifying the packaging (practical)

Plasma Instruments

Components of a Plasma Sensor

Analyzer selects a subset of particles to be measured.

Detector to amplify an event.

Analog signal processing to register an event.

Digital electronics to store/compress event data.

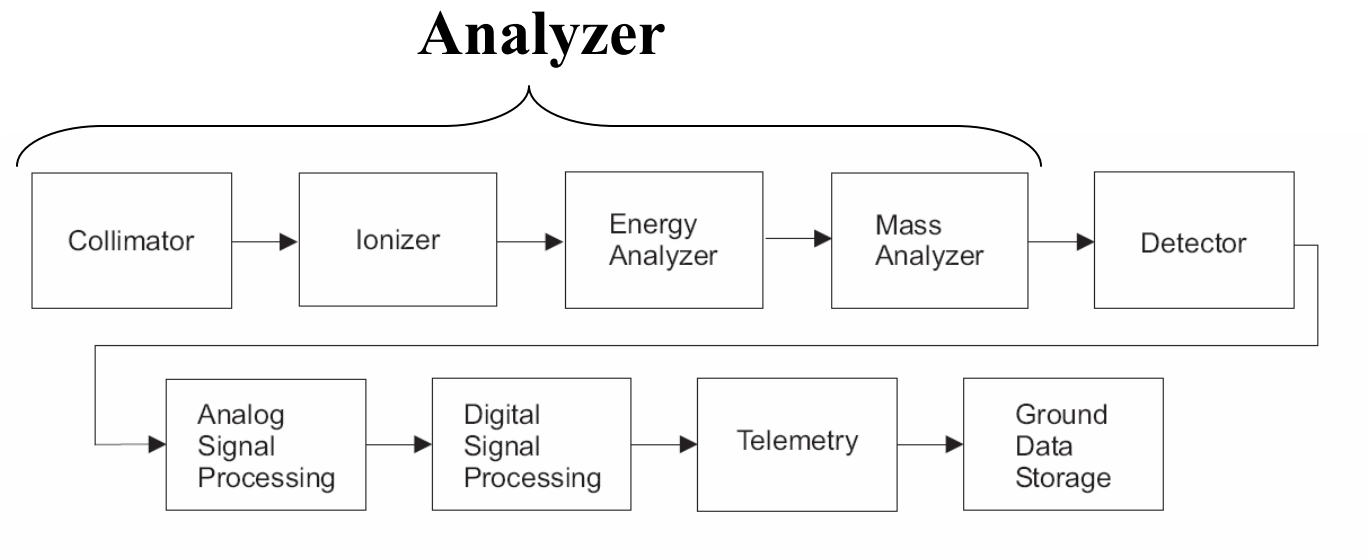

Detectors – Faraday Cups

Faraday cups are used to measure current.
Cannot detect individual particles.
Require large charged particle flux.
Very stable sensitivity over time.

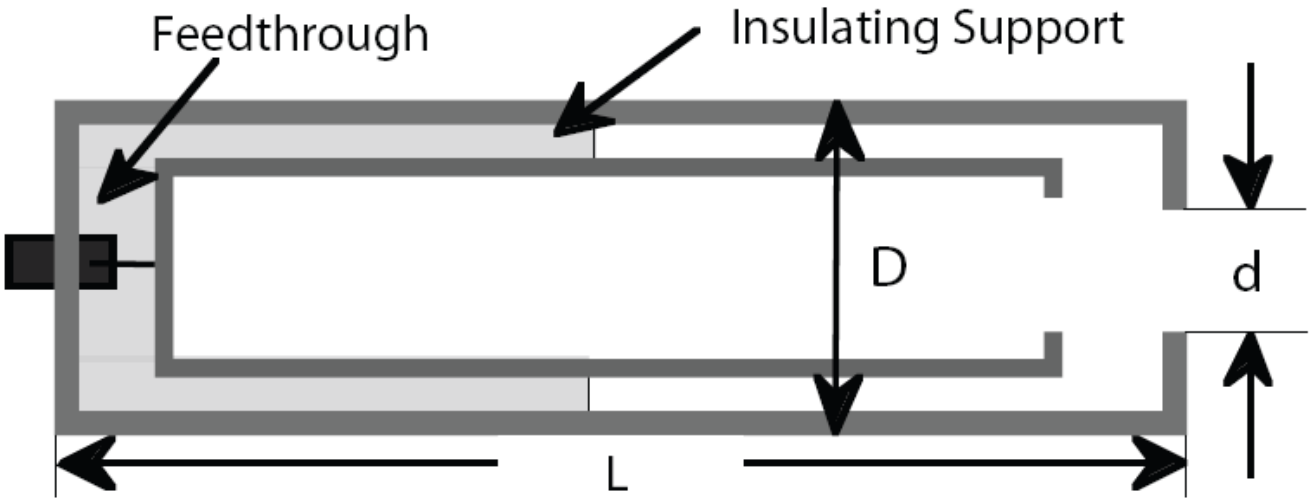

Figure 2.2: Schematic of Faraday cup as a particle detector.

Detectors – Dynode Multipliers

To detect a single particle requires a detector with gain.

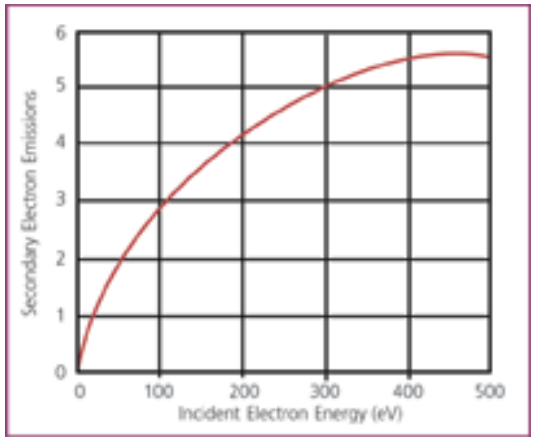

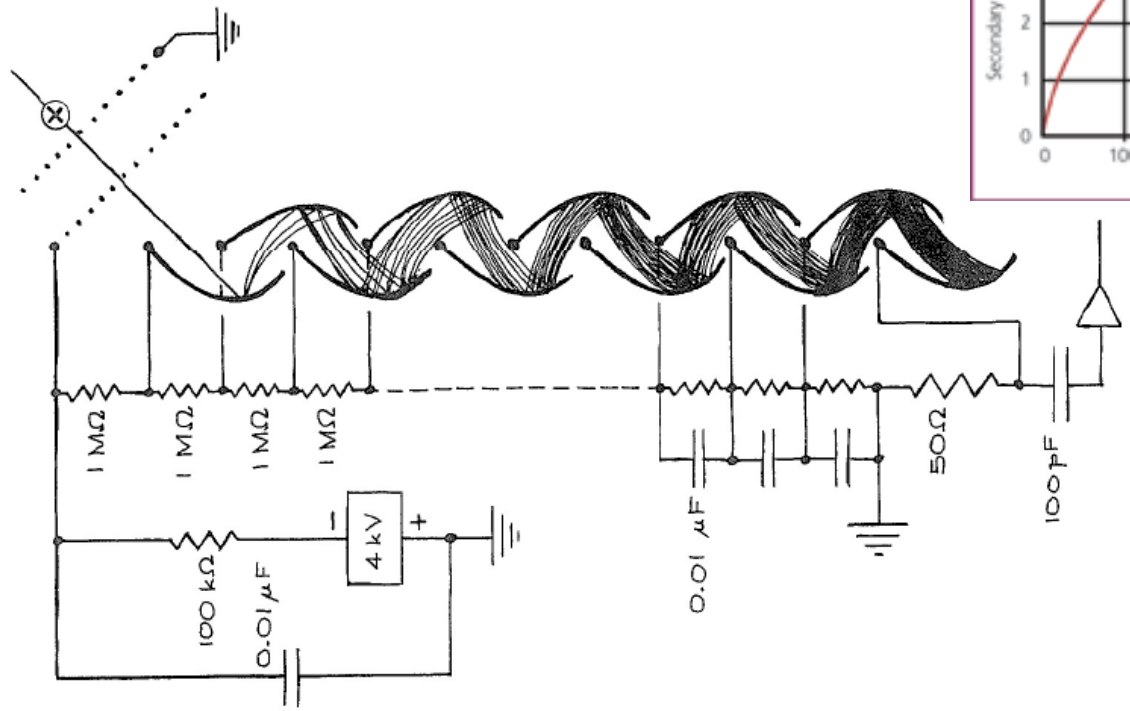

Figure 2.3: Open windowed discrete dynode multiplier with electrical connections to detect positive ions. Grids at the entrance of the multiplier prevent the escape of secondary electrons. From *Moore et al.* [1989].

Detectors – Channel Electron Multiplier (CEM)

The channels are curved to prevent ion feedback. Tube diameter ~1-2 mm. CEM diameter ~3 cm.

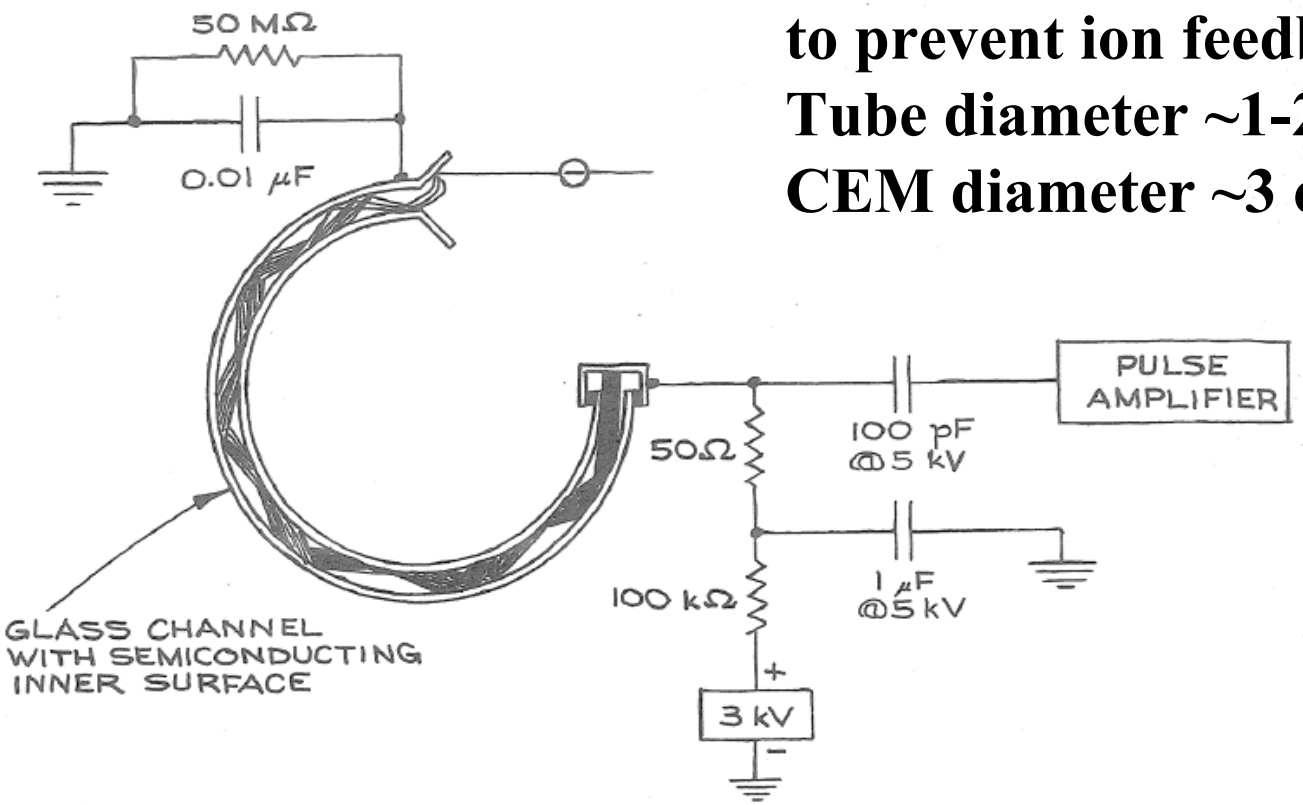

Figure 2.4: Continuous electron multiplier with electrical connections to detect electrons. From *Moore et al.* [1989].

Detectors – Microchannel Plates (MCPs)

Channel diameter ~5-25 um, Plate diameter up to ~10 cm.

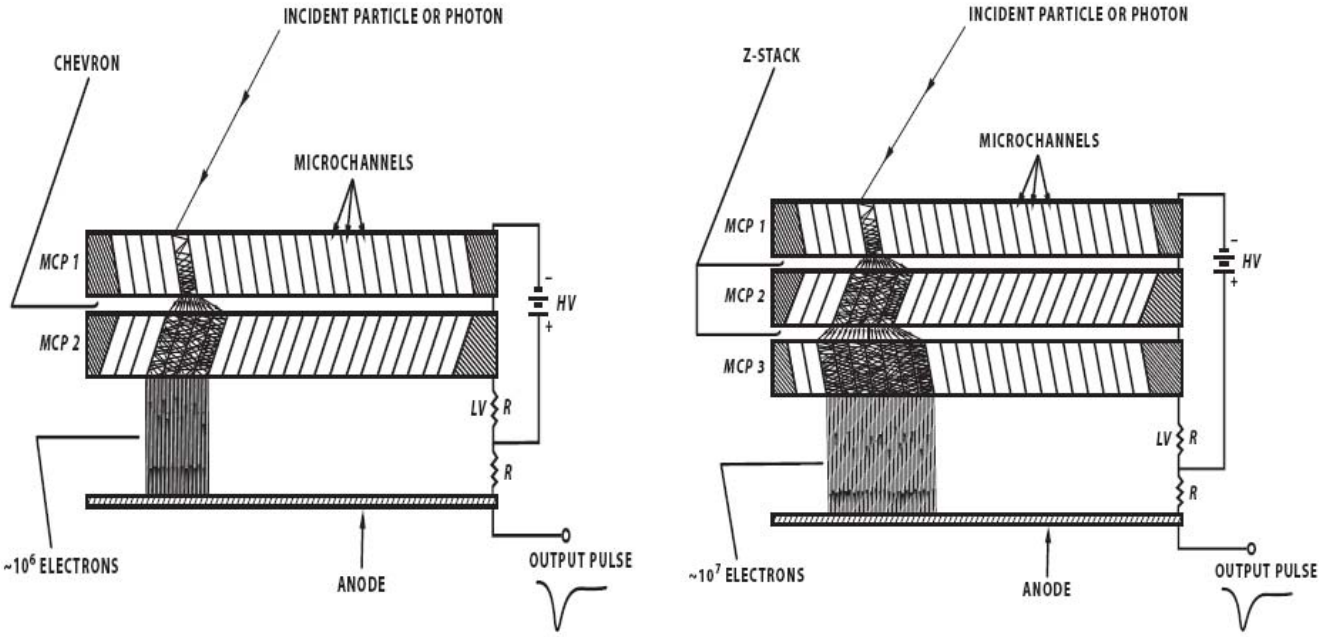

~1 kV per plate

Figure 2.9: Schematic drawing of MCPs in chevron (left) and Z-stack (right) configuration. The LV next to the resistor between the back of MCP and anode is to indicate that the voltage drop across this resistor is small. Generally, the potential difference between anode and the back of the MCP is desired to be 50–100 V). The resistance is only about 2–4 % of the MCP resistance. Nearly all the MCP current flows through this resistor. The resistor from the anode to the HV carries only a tiny current from the charge pulses and has virtually no voltage drop. The anode resistor bleeds off the current since the preamplifier is generally capacitively coupled.

Detectors – Microchannel Plates

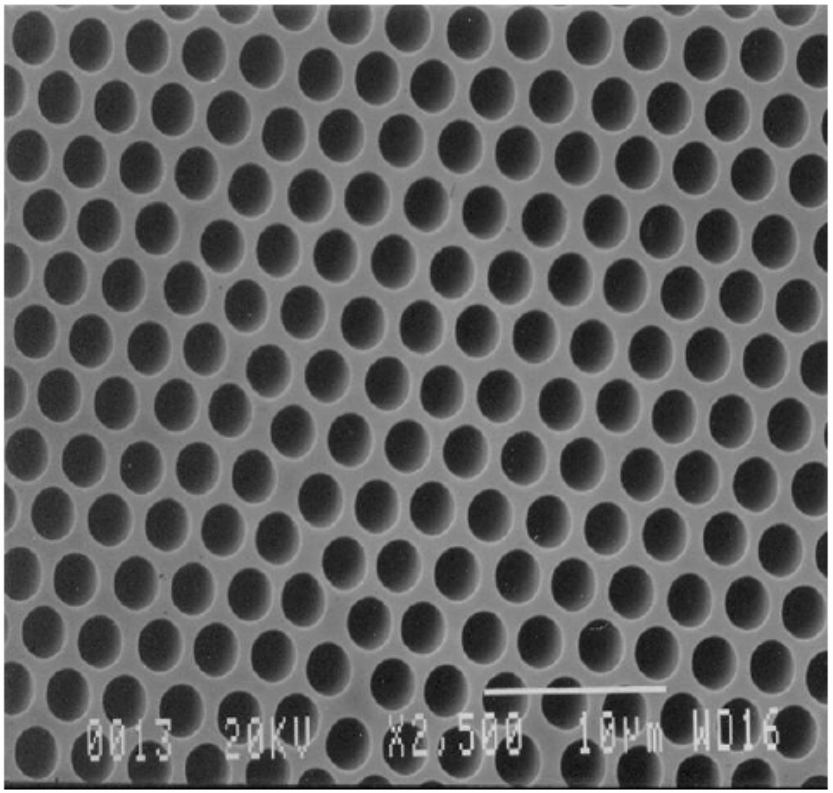

Figure 2.8: Photo of a microchannel plate surface. Figure courtesy of Burle Industries, Inc.

Detectors – Bias Voltage

The change in count rate near threshold reflects the shape of the MCP pulse height distribution.

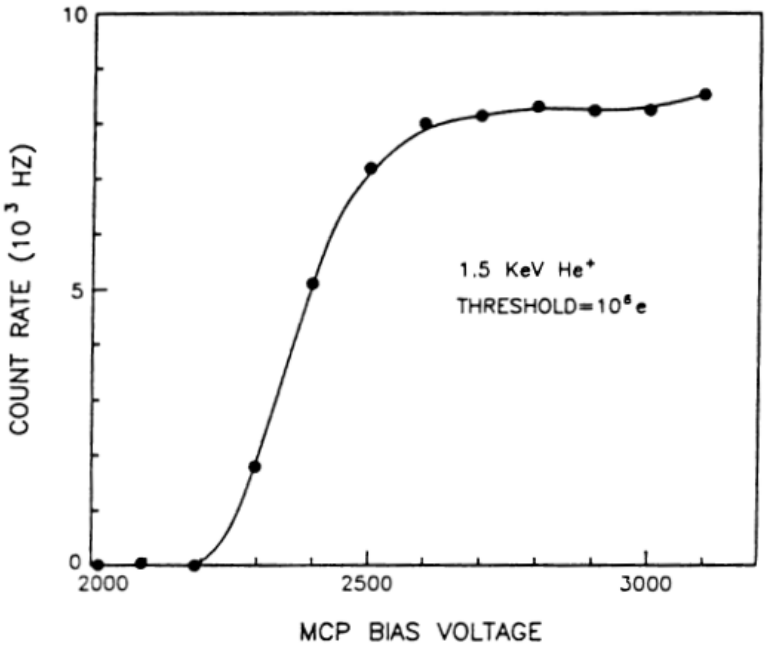

Figure 2.10: Akebono suprathermal ion mass spectrometer flight microchannel plate response as a function of MCP bias voltage. The nominal saturated gain was measured to be 10^7 and the threshold for the pulse height discrimination was set at 10^6. The count rate plateau for 1.5 keV He^+ beam is reached near 2600 V and the plateau is relatively flat up to 3000 V, where the MCP noise begins to make a significant contribution to the count rate. From *Whalen et al.* [1990].

Detectors – Pulse Height Distributions

Chevron – 2 MCPs

Z-Stack – 3 MCPs

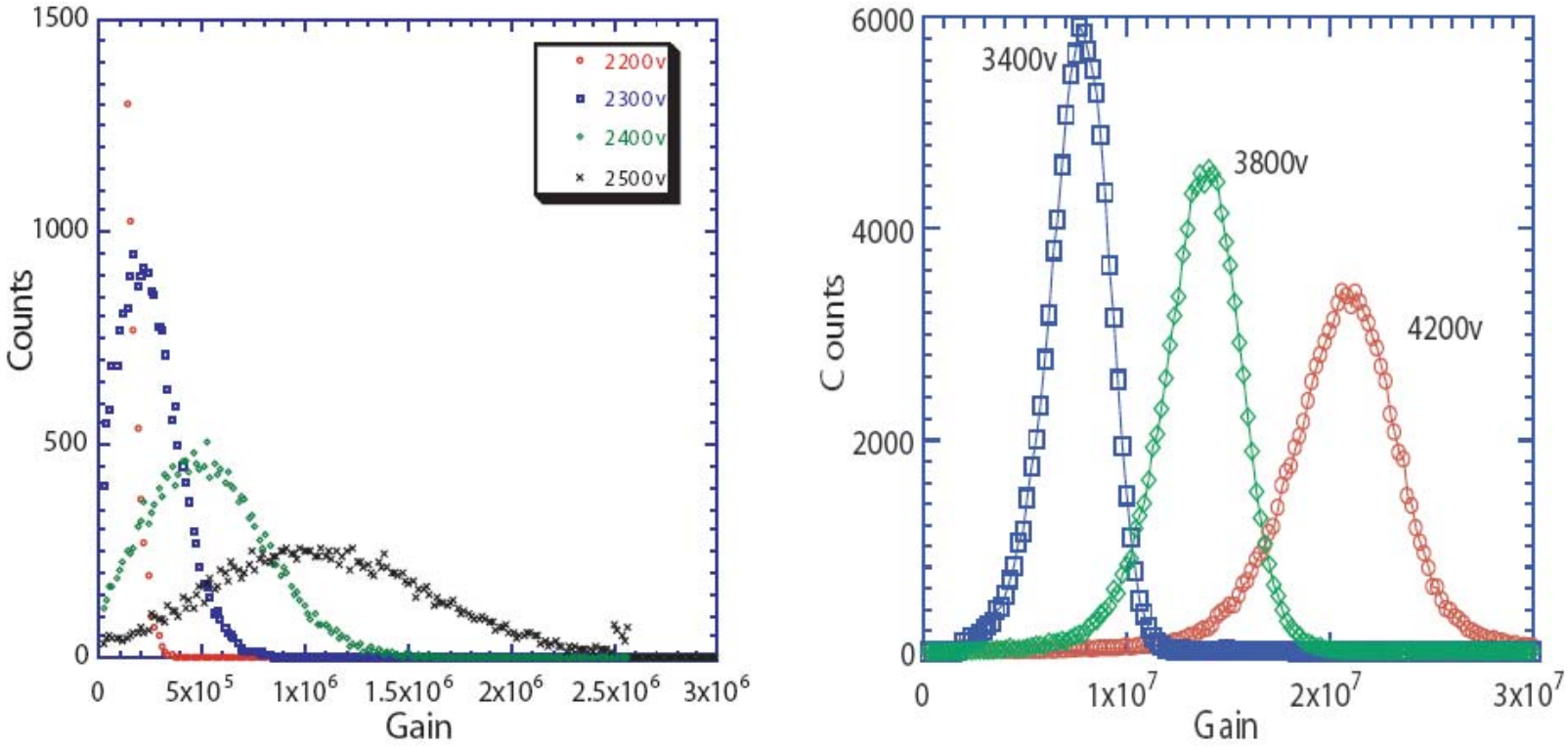

Figure 2.11: Pulse height distributions for Photonis 6 μm chevron pair (left) and Photonis 12 μm Z-stack (right). Figure courtesy of O. Siegmund.

Detectors – Electron Detection Efficiency

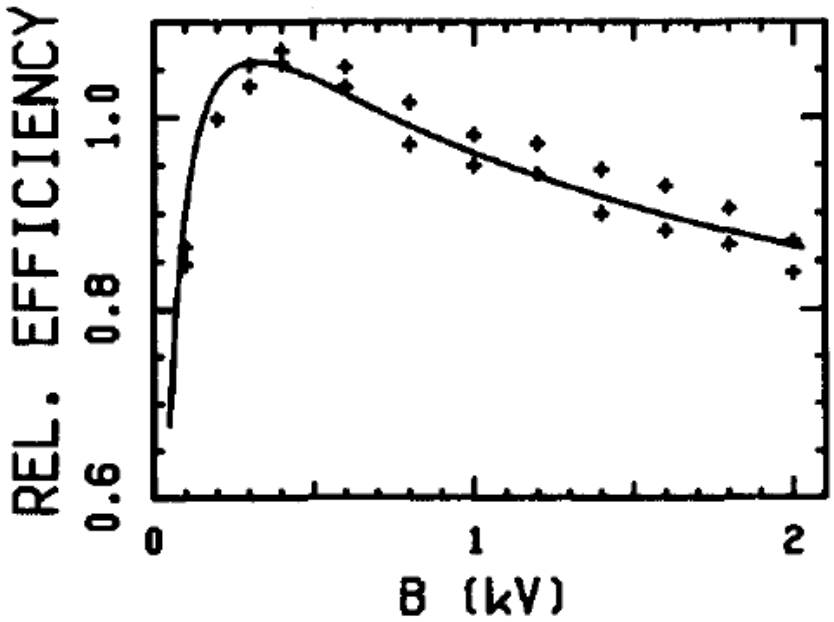

Figure 2.17: Variation of the relative detector efficiency $\epsilon(E, B)$ with the acceleration voltage B for electrons of energy 4 eV. The energy of the electron when it strikes the MCP surface will be $(4 + B)$ eV. Efficiency at 200 V is normalized to unity. The pluses are experimental points and the solid curve denotes the theoretical fit according to Bordoni. From *Goruganthu and Wilson* [1984]; *Bordoni* [1971].

Detectors – Electron Detection Efficiency

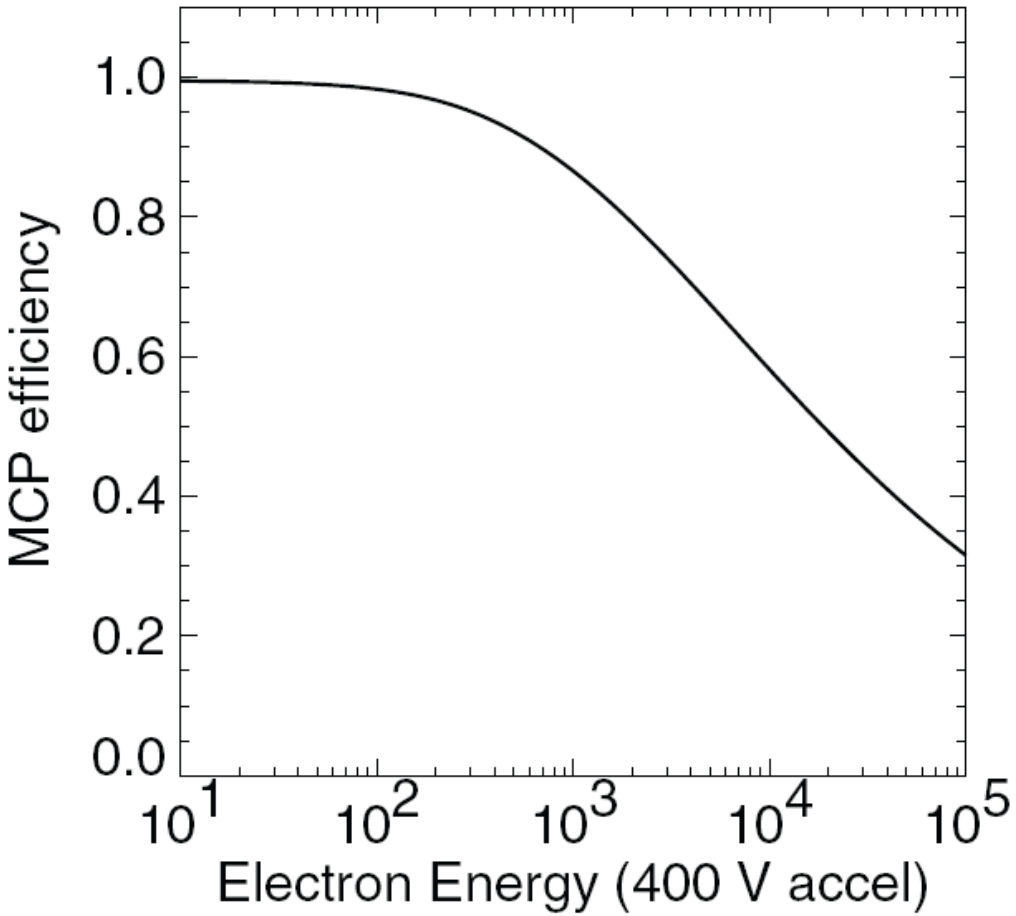

Figure 4.27: MCP energy dependent efficiency used to correct the Wind 3D Plasma electron measurements. The curve is based on published results by *Goruganthu and Wilson* [1984].

Detectors – Ion Detection Efficiency

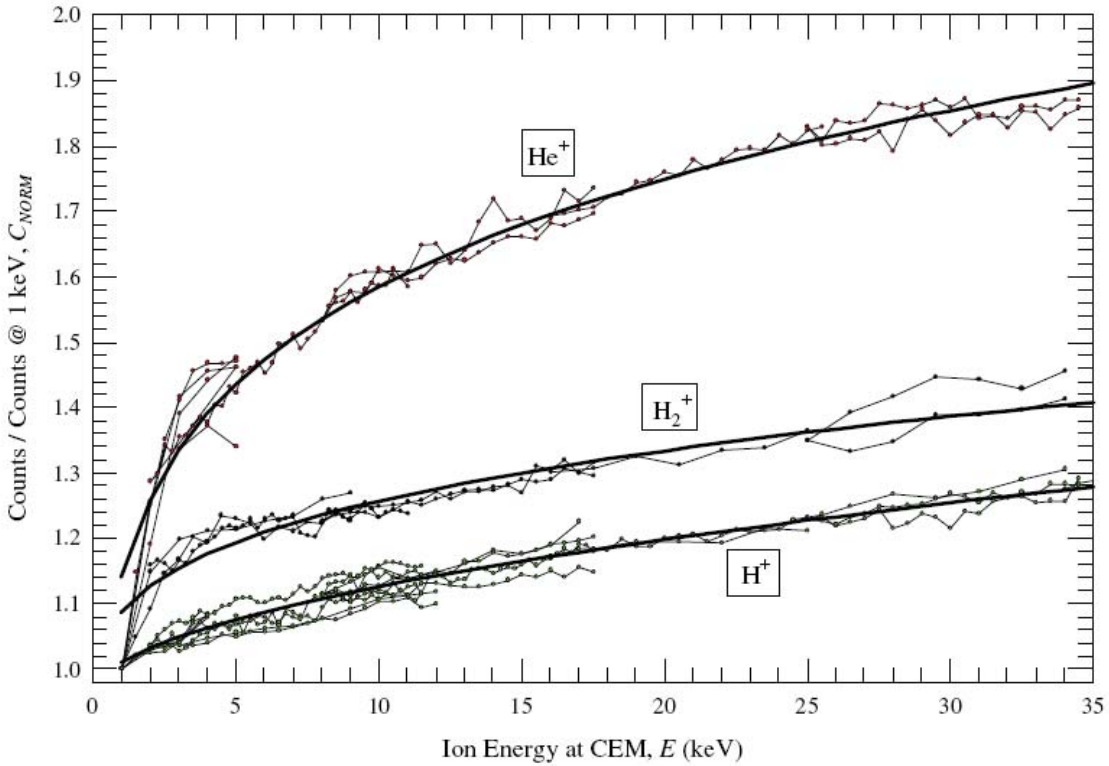

Figure 2.6: Comparison of relative channel electron multiplier detection efficiency of incident H^+, H_2^+, and He^+ as function of energy. The relative efficiency is determined by the ratio of the count rate at beam energy "E" to the count rate at a beam energy of "1 keV", where the beam flux is independent of energy. Above ~2 keV, the CEM efficiency increases slowly with ion energy. Different ions manifest different energy dependent efficiencies. Figure courtesy of H. Funsten.

Detectors – Detection Efficiency w/ Angle

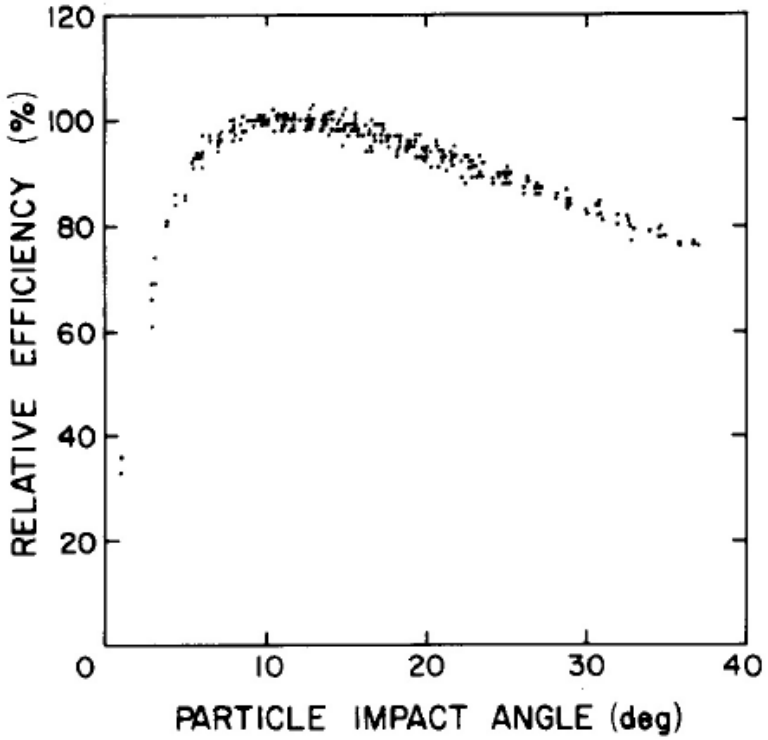

Figure 2.19: Relative detection efficiency as a function of the angle between the particle trajectory and the channel axis direction. The relative efficiency is found to be independent of particle species and energy. From *Gao et al.* [1984].

Detectors – MCP gain degradation

This initial gain degradation of MCP detectors is known as scrubbing. Surface contaminates, primarily water, are removed over time, reducing the secondary electron yield.

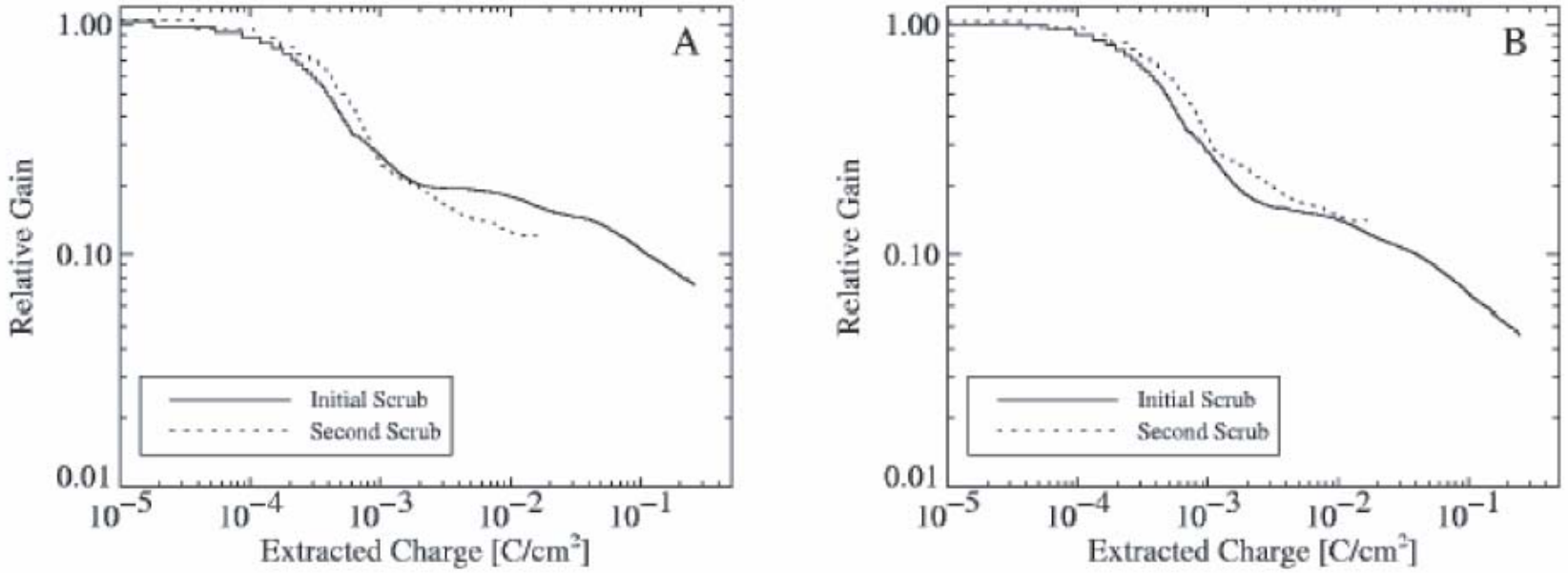

Figure 4.4: Relative gain as a function of charge extracted for the scrubs of the two MCP segments A and B of the COS-FUV01 instrument on HST. From *Martin et al.* [2003].

Detectors – MCP gain degradation

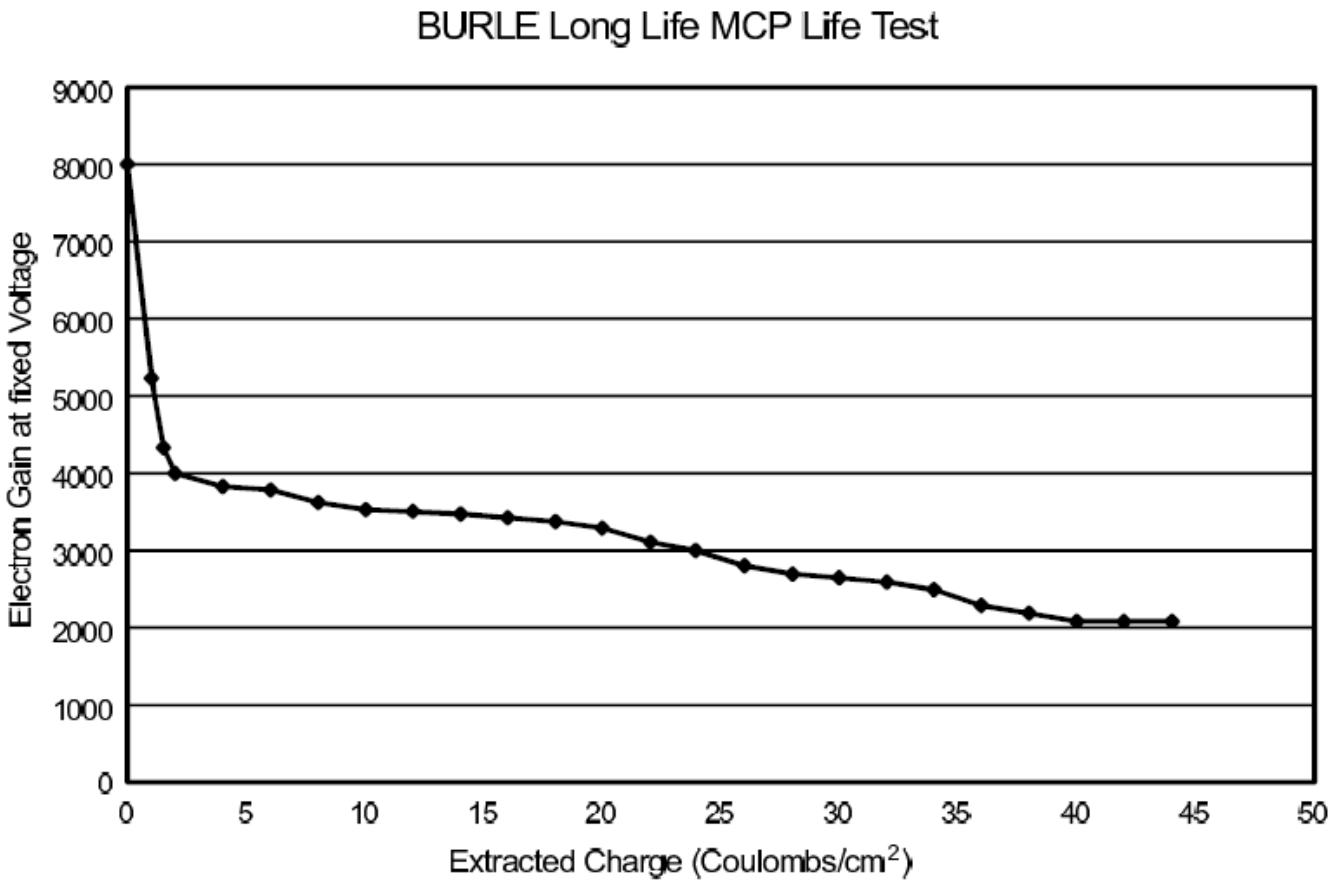

Figure 4.2: MCP gain vs. extracted charge.

Analog Signal Processing – Discrete Anodes

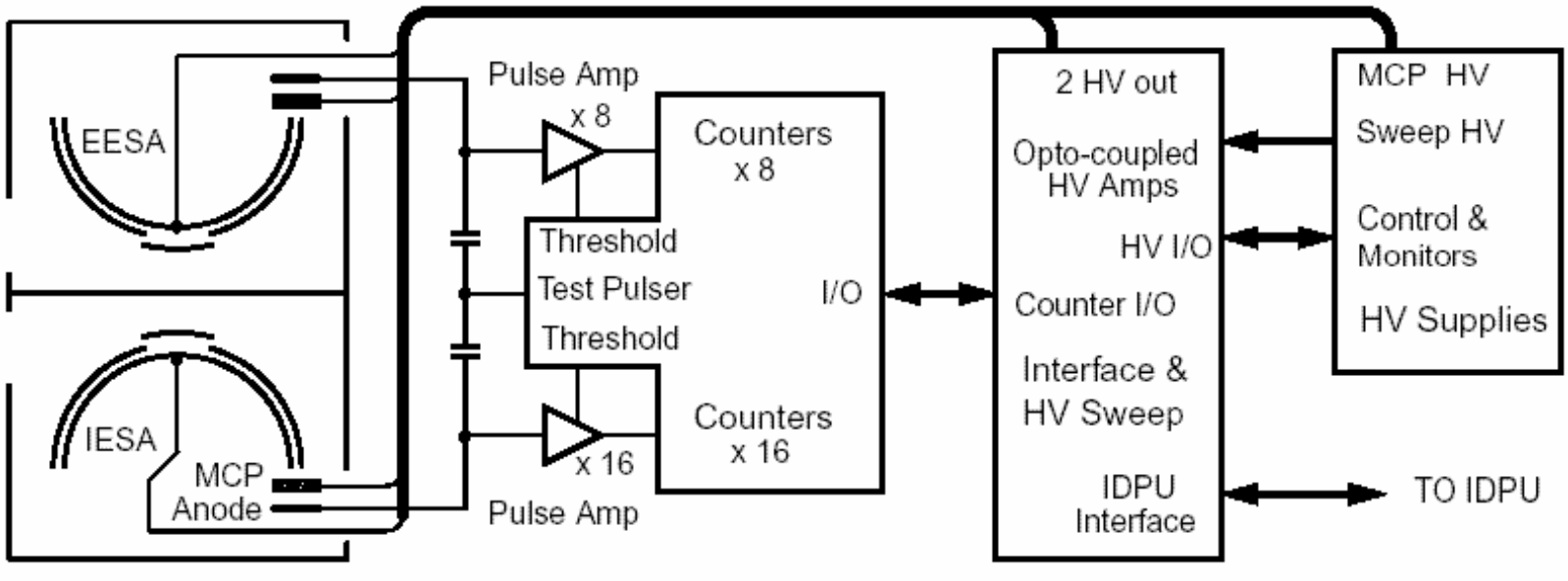

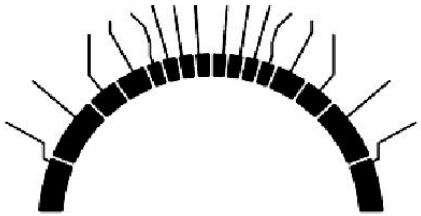

Ion ESA
16 Anodes

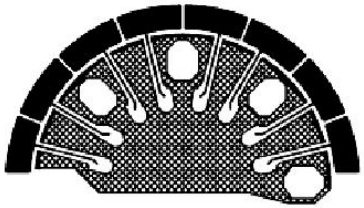

Electron ESA
8 Anodes

Discrete anodes provide highest counting rates with modest angle resolution.

Analog Signal Processing

THREE TYPES OF POSITION SENSING PARTICLE DETECTORS

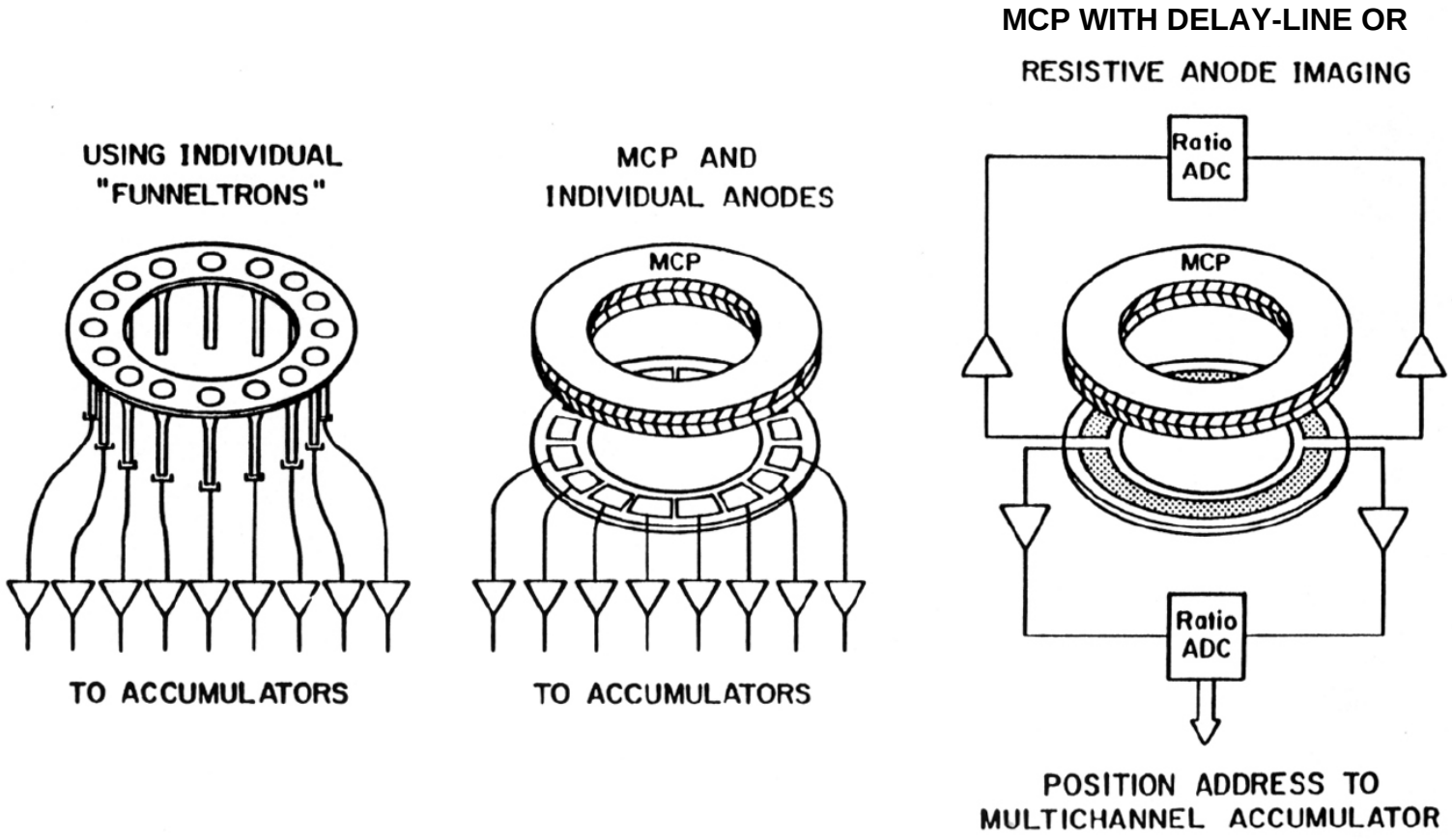

Analog Signal Processing – Delay Line

Serpentine signal line must be impedance matched.

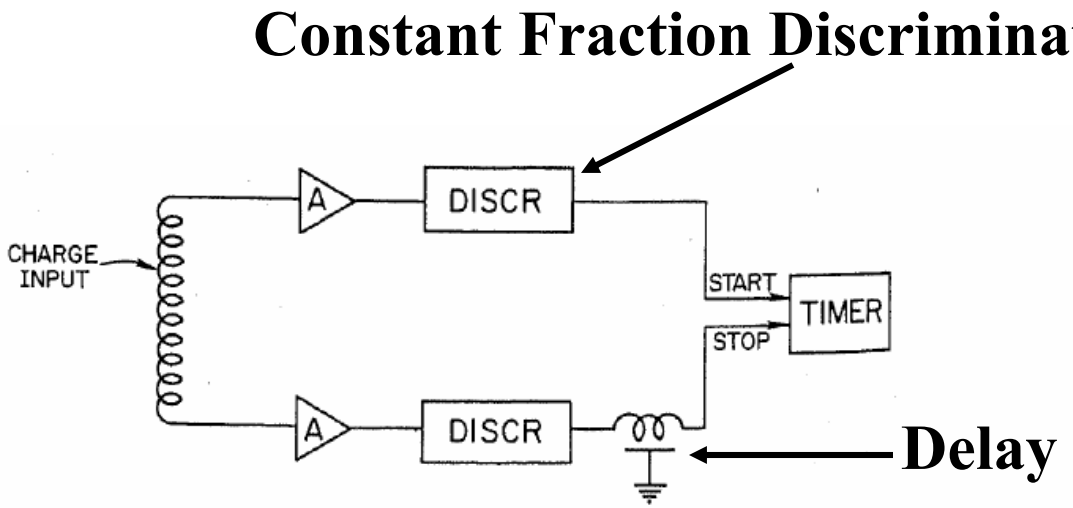

Figure 2.13: Schematic drawing of delay line position sensitive detector. A localized charge pulse collected by the delay line triggers START and STOP discriminators with a relative time delay that depends linearly on the centroid location of the event. From *Lampton et al.* [1987].

Continuous delay-line can provide finer angle imaging without requiring a large number of preamplifiers and their associated power.

Analog Signal Processing – Discrete Delay Line

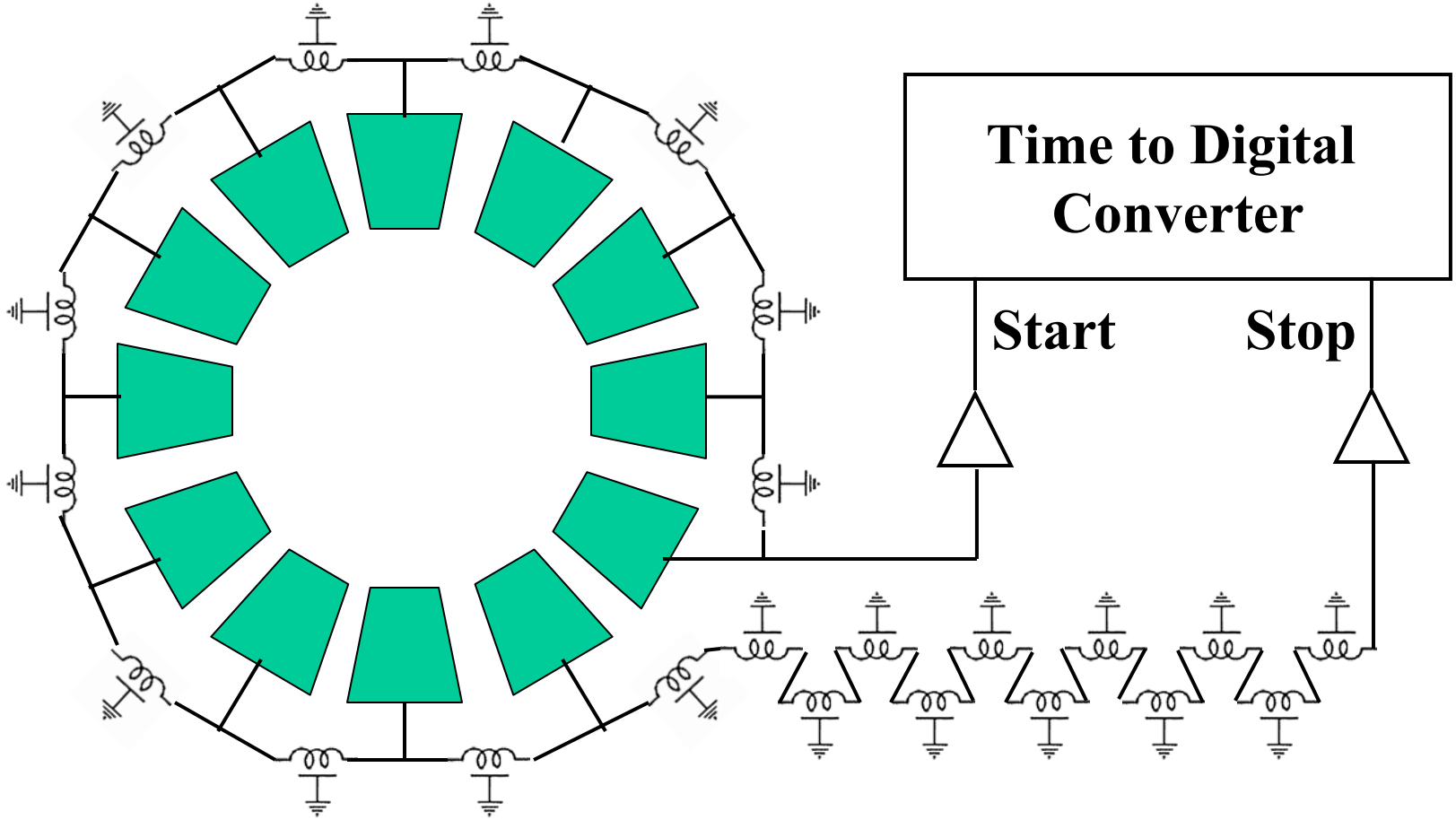

Discrete delay line can reduce the number of preamplifiers while providing fixed angle sector.

Analog Signal Processing – Resistive 2-D Imaging

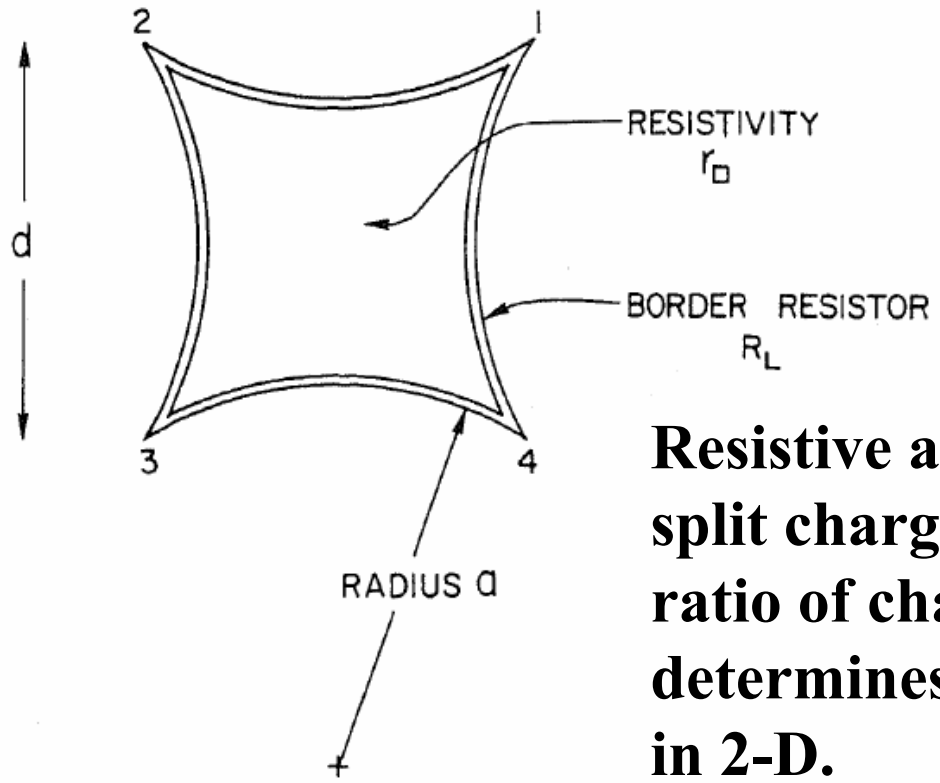

Resistive anodes can split charge, and the ratio of charge determines position in 2-D.

Figure 2.12: A circular arc terminated resistive anode. The anode is manufactured using thick-film resistor technique. Electrical connections are made at the four corners. The position of the detected event is computed from the ratio of charge pulse amplitudes. From *Lampton and Carlson* [1979].

Analog Signal Processing – Wedge & Strip

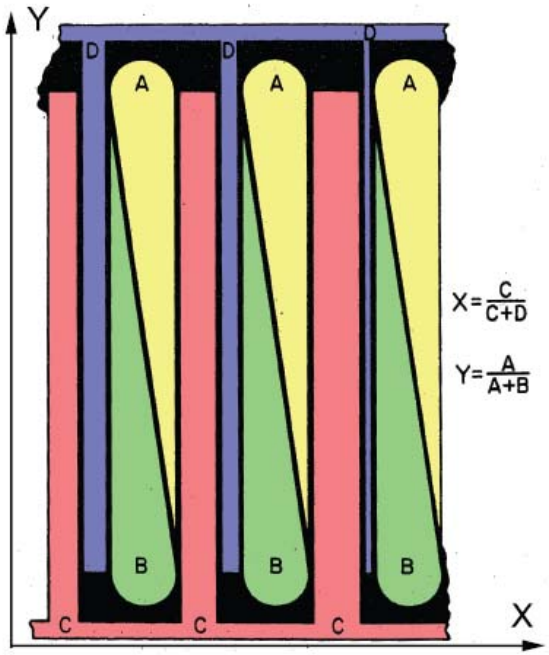

Wedge and Strip anodes can split charge, and the ratio of charge determines position in 2-D.

Figure 2.14: A portion of a four-electrode wedge and strip anode pattern. Black regions are insulators and white areas are conductors. All wedges marked "A" are connected together by a common conductor located beneath the anode plane; similarly the "B" wedges are connected to a second common conductor. The ratio of these two signals depends on the y coordinate of the event. Simultaneously the pairs of strips "C" and "D" are used to determine the x coordinate of the event, since the relative widths of these strips vary linearly with x. The coding is nearly distortionless if the size of the deposited charge footprint is somewhat larger than the distance between quartets. The formulae shown are coordinate recovery algorithms appropriate for this geometry. Adapted from *Martin et al.* [1981].

Analyzers – Retarding Potential

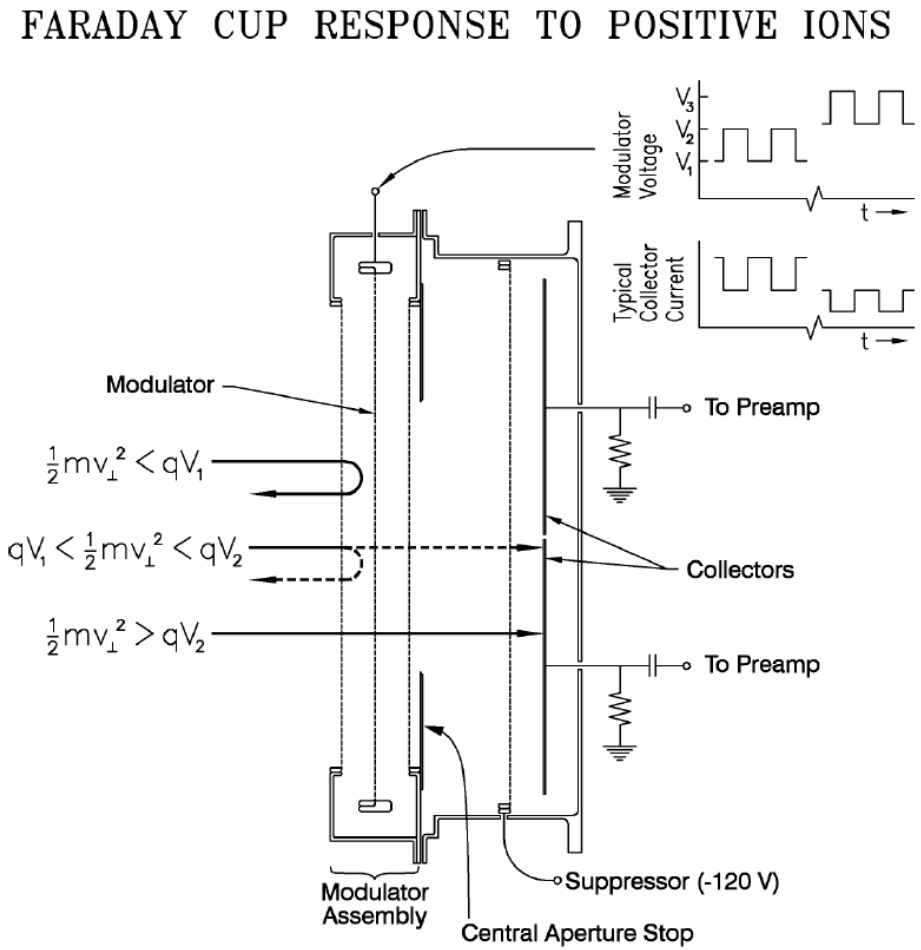

Figure 2.23: A schematic cross-section of the Wind FC instrument along its symmetry axis showing the entrance aperture, the modulator assembly, the limiting aperture, the suppressor grid, and the collector plate (oriented perpendicular to the page), which is split into two semicircular plates.

Fixed voltage retarding grid provides integral measurement with sharp low energy cutoff.

Modulated retarding grid and filtering can provide a differential measurement of flux.

Analyzers – Cylindrical Electrostatic

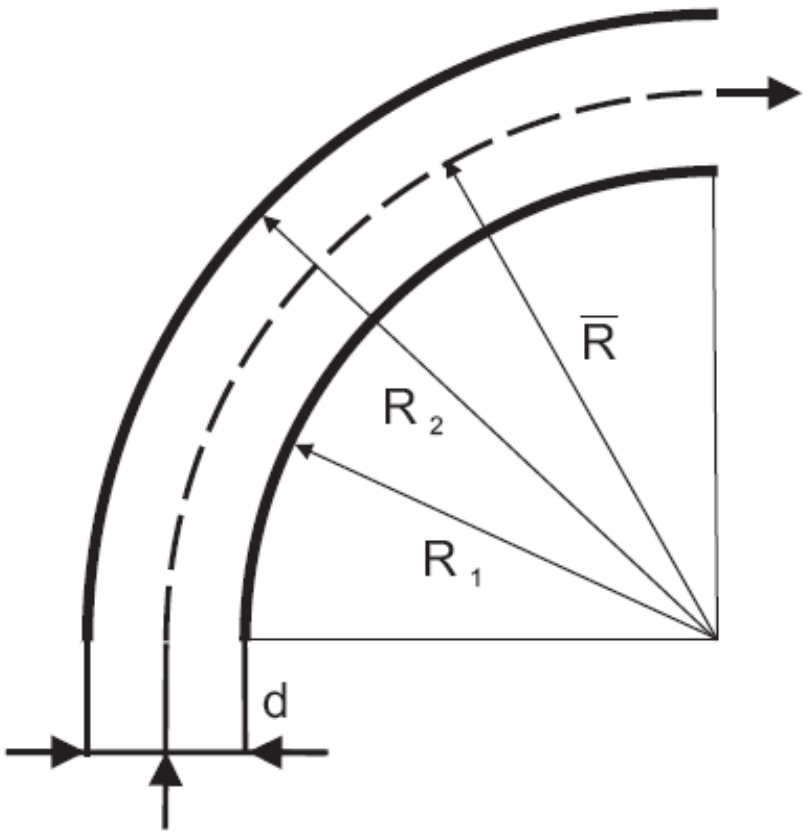

Figure 2.27: Cylindrical electrostatic analyzer.

For trajectories without out-of-plane velocity.

$$E = \frac{q(V_2 - V_1)}{2 \ln \frac{R_2}{R_1}}$$

Energy Constant = E/qΔV
= R/2ΔR

$$\Delta E \cong qV/2\Delta R$$

$$\Delta\alpha \cong \Delta R/\bar{R}$$

Analyzers – Electrostatic Spherical

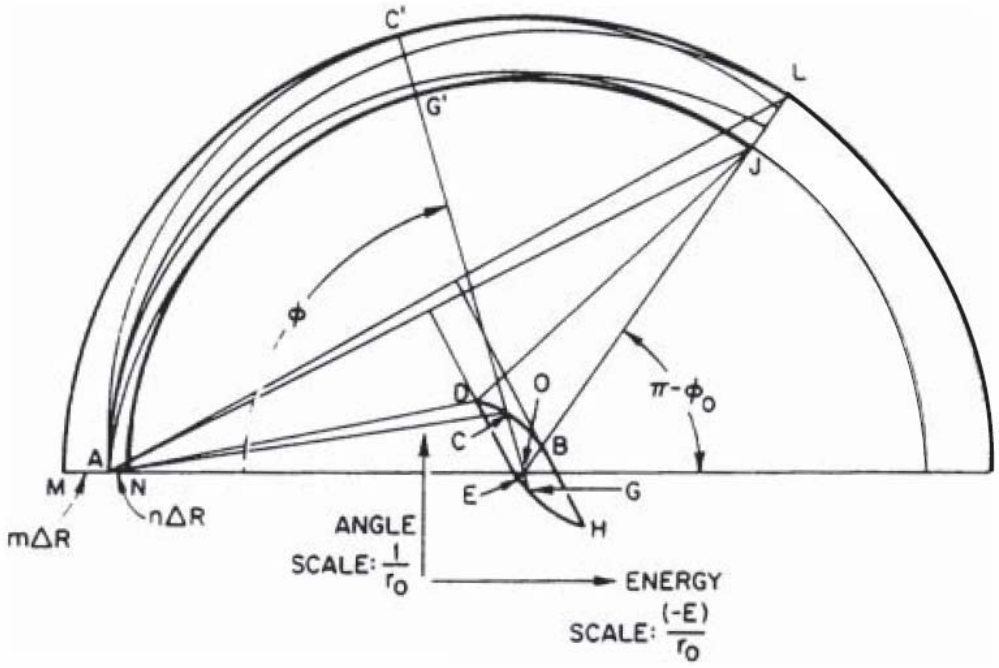

Figure 2.28: Locus of centers of transmitted particle trajectories in a spherical analyzer of arbitrary central angle ϕ_0 for an arbitrary point of incidence A. C′ and G′ are points of tangencies of trajectories with analyzer plates and J and L are points of intersection with the analyzer walls at the exit aperture defined by the angle ϕ_0. The locus is the total area within the curve DEGHBCD. The vertical displacement of any point within this area from AO is linearly proportional to the angle of incidence α of the particle whose trajectory center is that point. The horizontal displacement of that point from the normal to AO at O is linearly proportional to the energy deviation ΔE of the particle from the energy giving the unperturbed circular orbit. Scale factors are as given in the figure. From *Paolini and Theodoridis* [1967].

Trajectories within spherical analyzers can be solved analytically, however fringing fields are not treated properly.

Analyzers – Spherical

Spherical analyzers provide angle focusing.

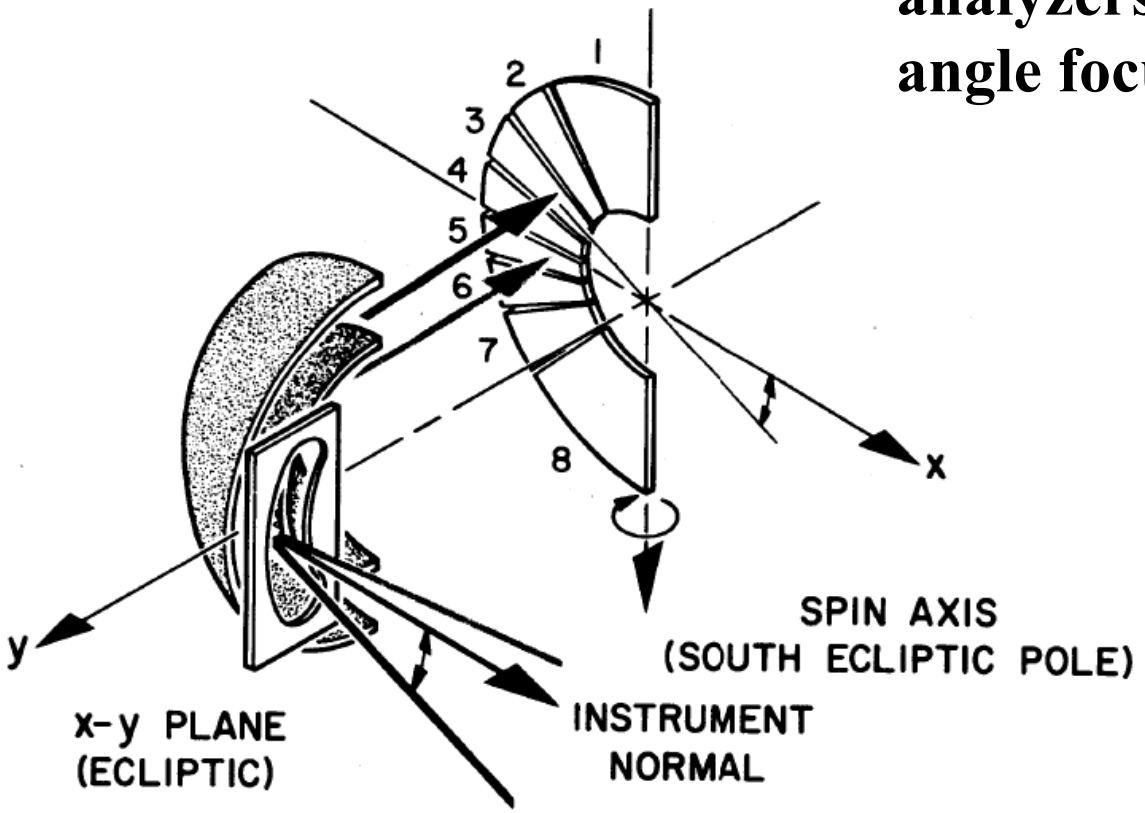

Figure 2.29: The Ames Research Center quadrispheric analyzer with sectored collector flown on the Pioneer-6 spacecraft. From *Scarf et al.* [1966].

Analyzers – Spherical Top-Hat

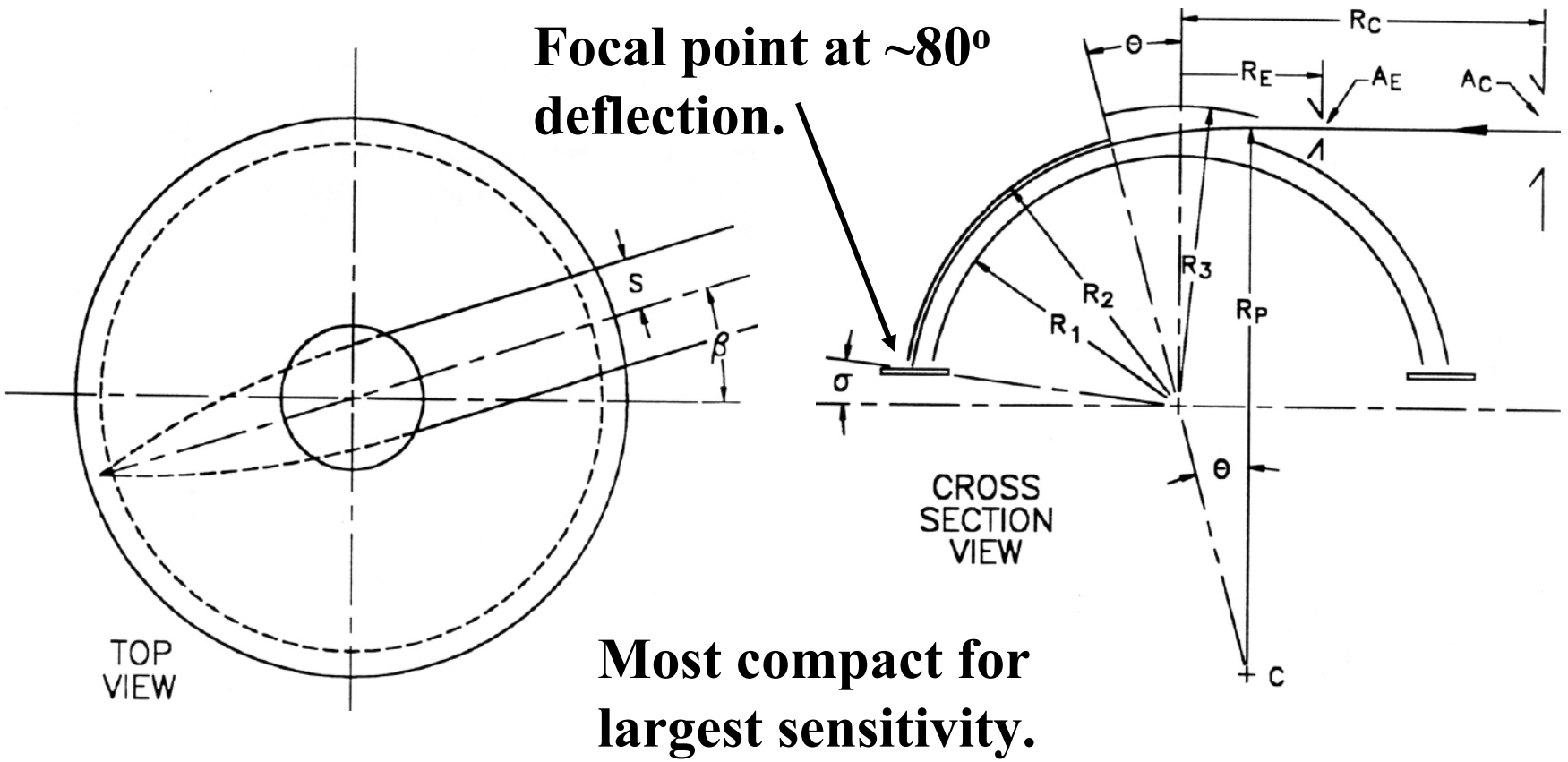

Figure 2.30: Top and cross-section views of spherical top-hat analyzer identifying principal parameters. A typical trajectory is shown. The particle's radius of curvature through the tophat region is approximately $2R_2$ with a center of curvature at C. From *Carlson and McFadden* [1998].

Analyzers – Top Hat Response

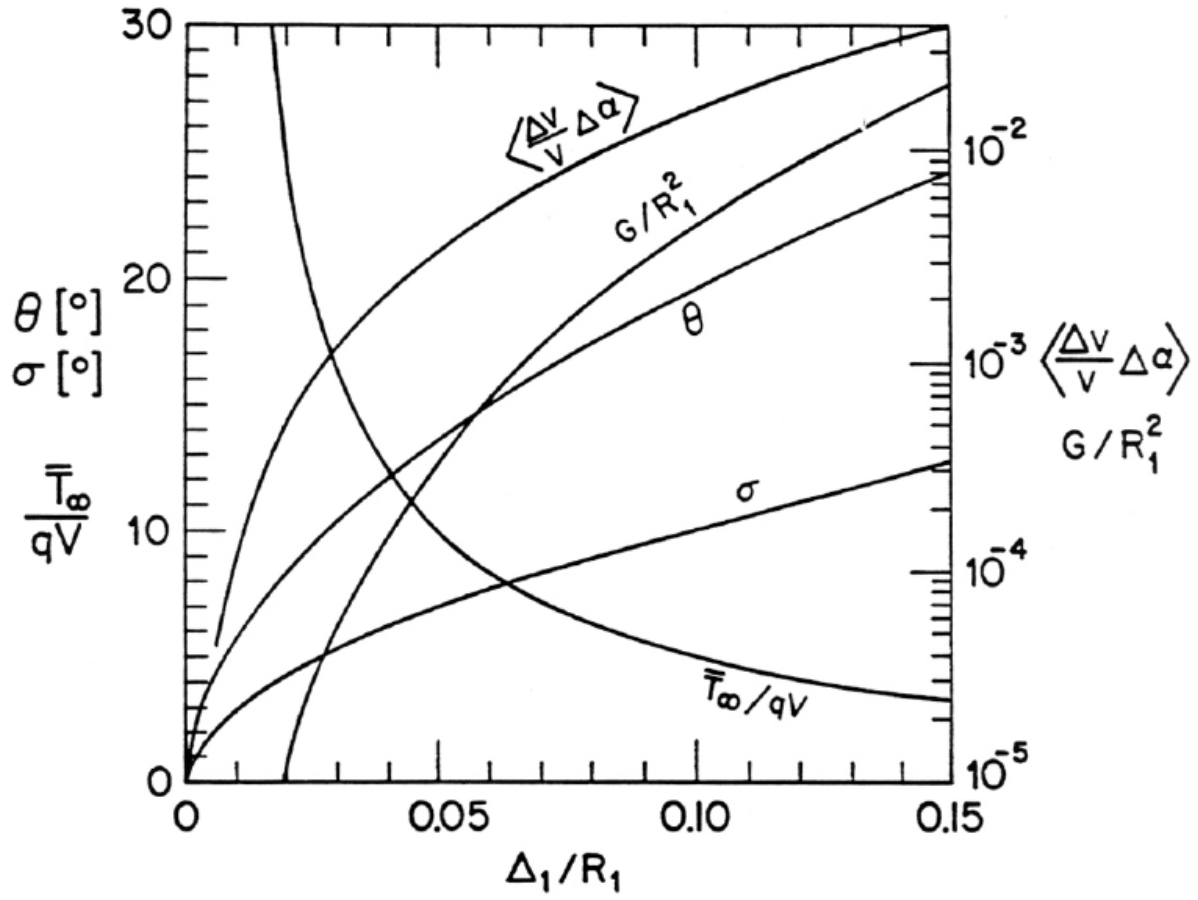

Top-hat analyzers have been characterized to allow optimization without resorting to simulations.

Figure 2.31: Summary of a spherical top-hat analyzer's performance parameter dependence on the ratio of the analyzer gap, $\Delta_1 = R_2 - R_1$, to the inner hemisphere radius, R_1. The indicated values for Θ and σ provide optimized angle imaging at the analyzer exit and zero average elevation angle "α" response at the analyzer entrance. Θ and $90° - \sigma$ are the entrance aperture opening and particle deflection angles, respectively, as defined in Figure 2.30. The other curves in the plot assume the optimal Θ and σ are used. T_∞/qV is the ratio of the average particle energy per charge far from the spacecraft to the applied inner hemisphere voltage, V, and is often referred to as the analyzer energy constant. For an analyzer with an acceptance area A and viewing a solid angle Ω, the normalized velocity geometric factor, $G/R_1^2 = G(v)/R_1^2 = A\Omega(\Delta v/v)/R_1^2$, and analyzer resolution, $(\Delta v/v)\Delta\alpha$, are illustrated in the remaining curves. Note that the more commonly used energy geometric factor, $G(E) = A\Omega(\Delta E/E)$, is equal to $2G(v)$ since $\Delta E/E = 2\Delta v/v$. These curves provide a useful starting point for selection of analyzer parameters (Δ_1, Θ, σ) to match the required sensitivity (G) and resolution ($\Delta v/v$, $\Delta\alpha$). From *Carlson and McFadden* [1998].

Analyzers – Toroidal

For spherical analyzers the deflection and symmetry radius are the same and parallel velocity particles focus after 90 degrees of deflection.

For cylindrical analyzers the symmetry radius is infinite and parallel velocity particles never focus.

Toroidal analyzers have the symmetry radius different from the deflection radius. By choosing the symmetry radius larger than the deflection radius, parallel velocity particles will focus after >90 degrees deflection.

By carefully choosing the ratio of these radii, one can select the focal point of the analyzer.

Analyzers - Toroidal

Toroidal design with "flat-top" transition. However, flat surfaces are more susceptible to sunlight UV scattering.

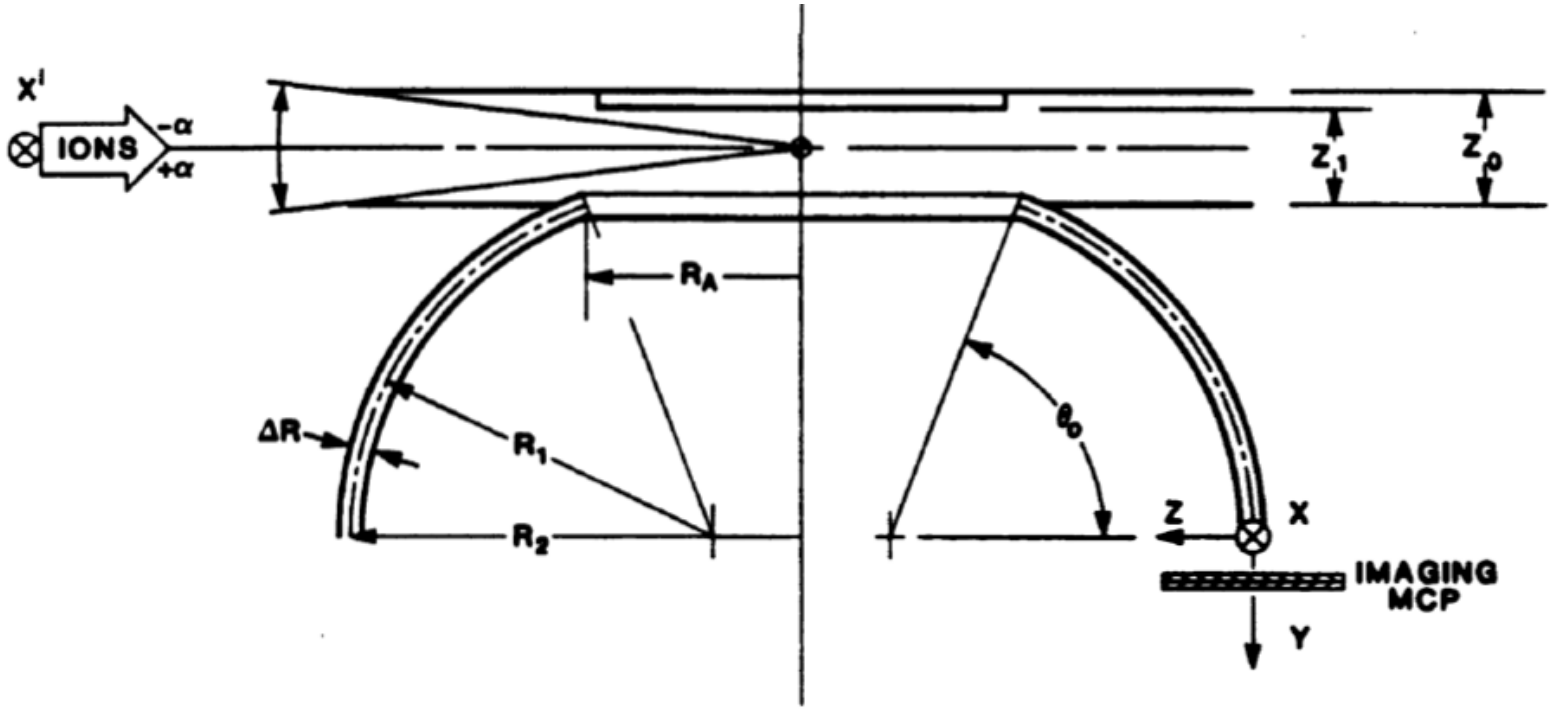

Figure 2.32: Schematic diagram of a toroidal top-hat analyzer. In this case the inner toroidal plate is truncated at $\theta = 75°$ by a flat surface. This lower surface is matched by an upper flat plate that forms part of a circular collimator and deflector. From *Young et al.* [1988].

Analyzers – Toroidal Continuous

Toroidal designs with "spherical-hat" avoid sunlight problems.

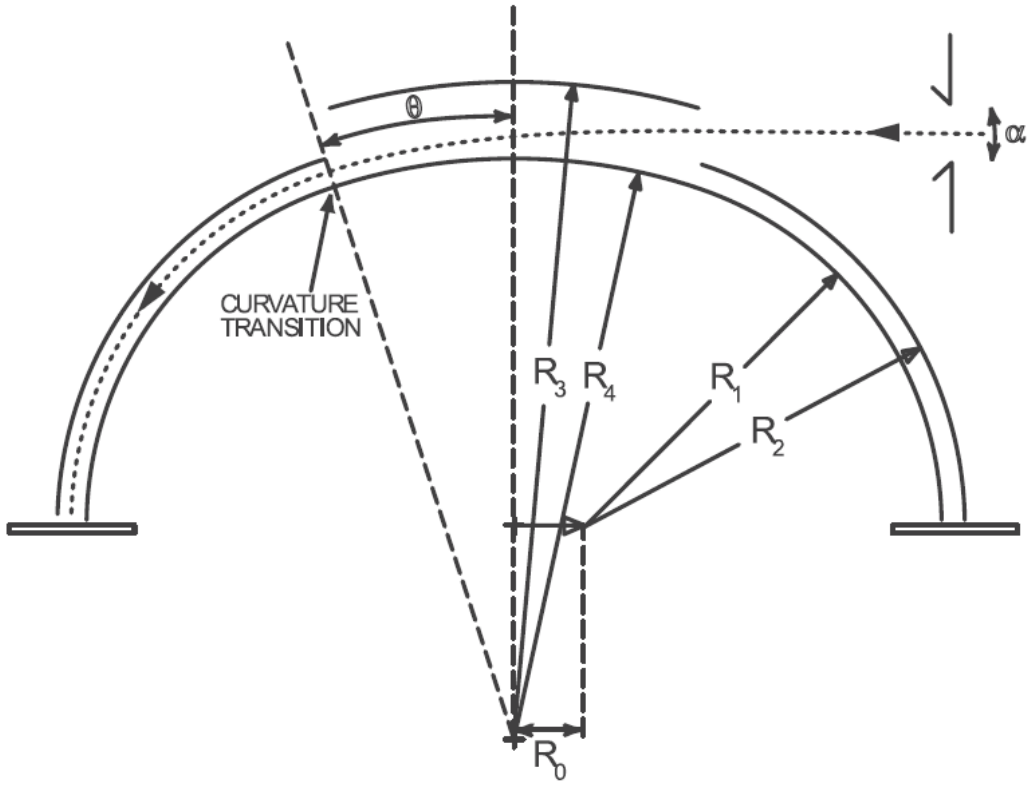

Figure 2.33: Schematic diagram of a toroidal top-hat analyzer with a spherical top-hat. The radius R_4 is chosen to provide a continuous curved surface by matching slopes at the interface between different curvatures. From *Carlson and McFadden* [1998].

Toroidal designs allow the imaging focal point to be located beyond 80° of deflection.

Analyzers – Magnetic Ion

Deflection determines ion momentum.
Broom magnet is used to remove electrons

Energy determined by SSDs.

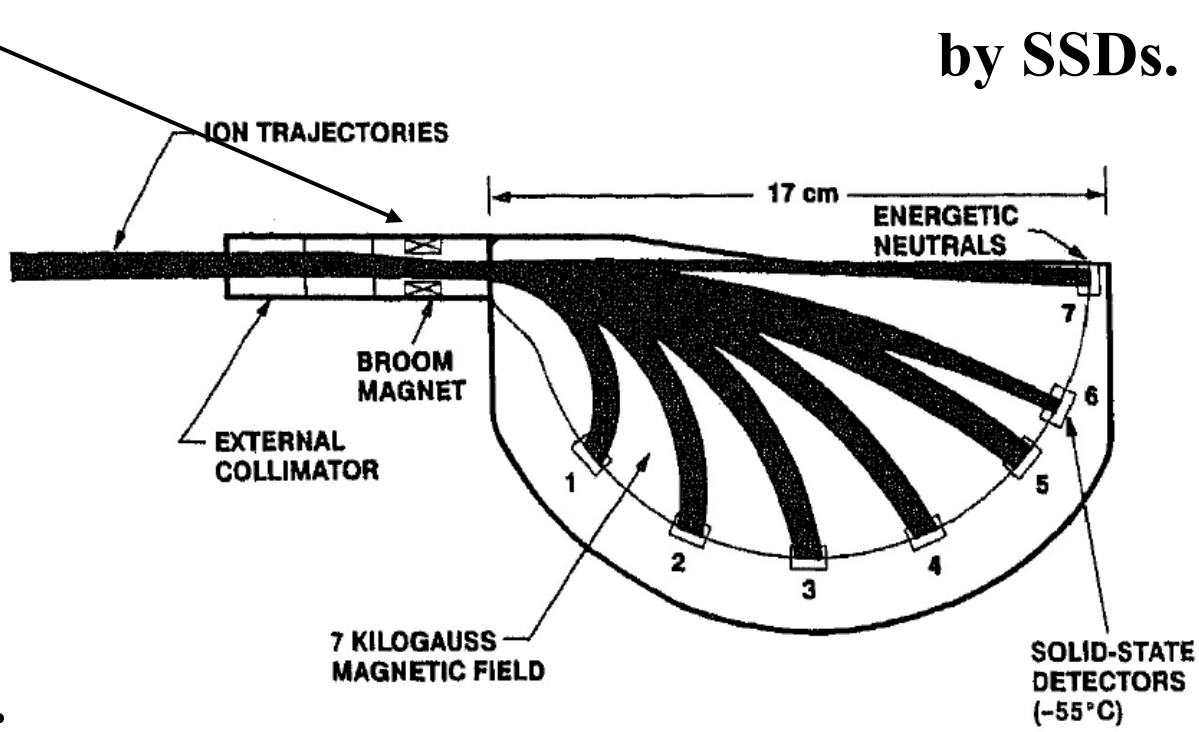

Momentum and energy allow determination of composition.

Figure 2.35: Principle of operation for IMS-HI is based on ion momentum, mass defect, and energy analysis using an array of cooled solid-state detectors. The magnet is shown in the lower portion of the figure and the ion optics in the upper portion. From *Voss et al.* [1992].

Analyzers – Magnetic Electron

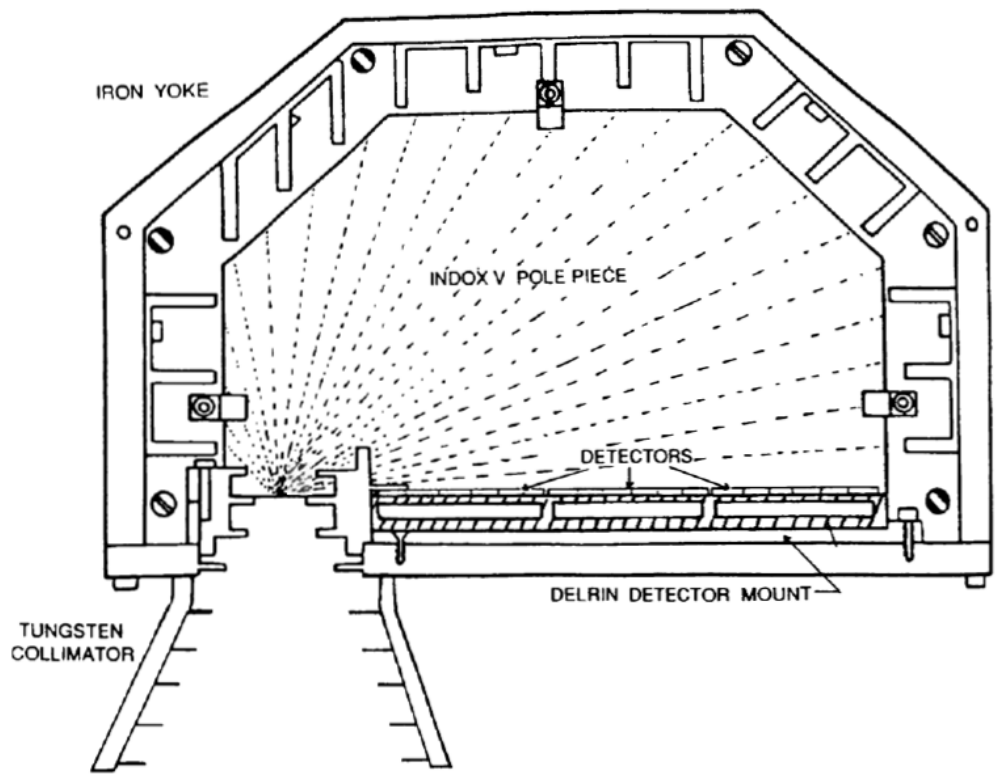

Figure 2.36: Schematic of the CRRES medium electron A (MEA) instrument. The disk-loaded collimator and the fins and ridges (indicated by dashed lines on the pole piece) in the housing structure ensure that an electron must undergo numerous scatterings in a low Z material in order to reach a detector unless its trajectory lies entirely within the collimator acceptance zone. From *Vampola et al.* [1992].

Electron spectrographs have limited energy range.

Internal scattering limits spectral resolution.

Analyzers – Double Focusing

Double focusing provides the highest mass resolution for composition instruments. ESA and magnetic aberations can be made to cancel.

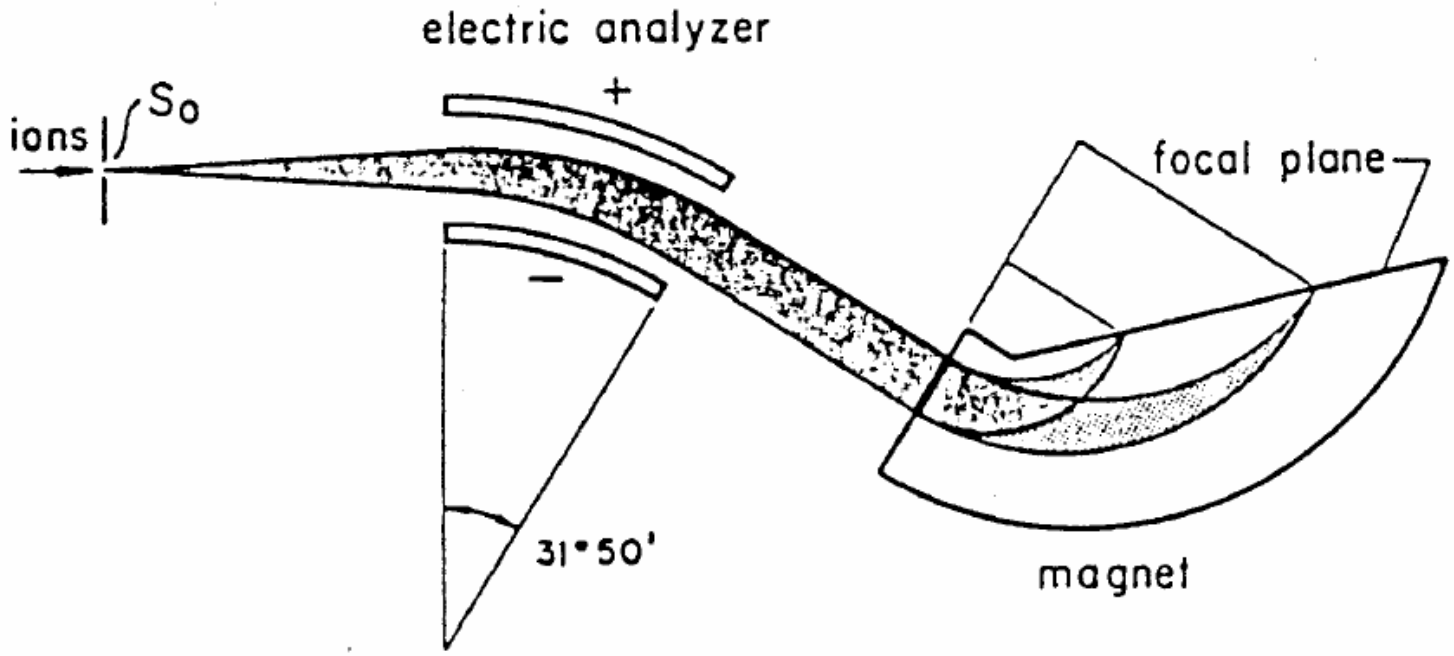

Figure 2.38: High-performance double focusing mass spectrometer of the Mattauch-Herzog design. From *Nier and Schuttler* [1985].

Analyzers – Time-of-Flight

Time of flight techniques allow ion velocity measurement without magnetic, thereby reducing mass.

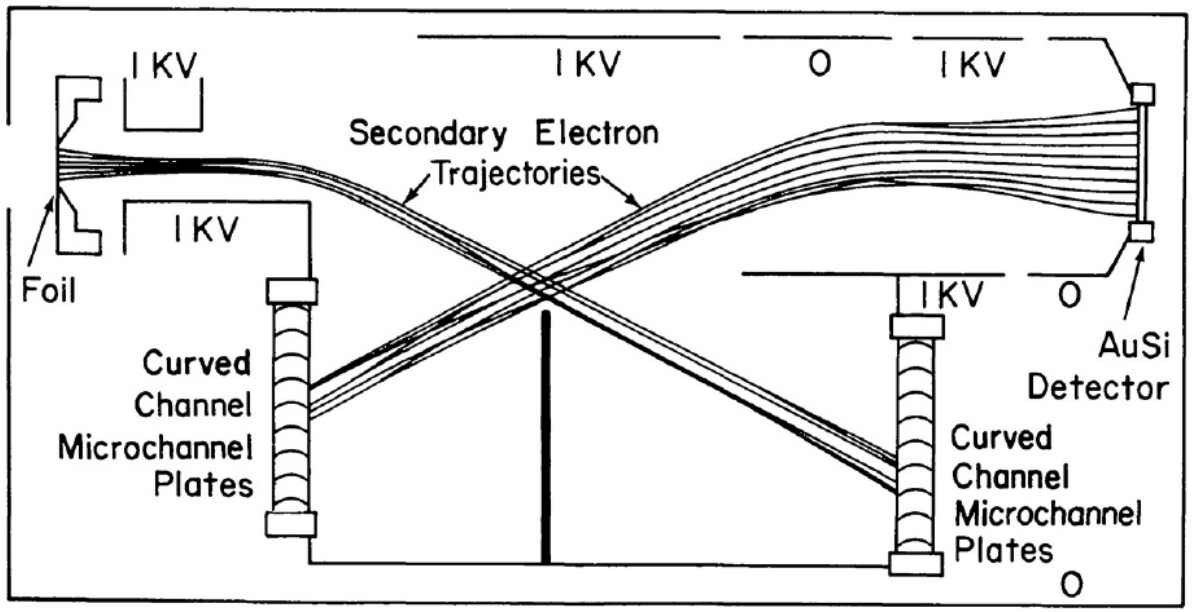

Figure 2.44: Schematic cross section of the Ulysses SWICS time-of-flight sensor showing computed trajectories of secondary electrons emitted from the carbon foil and the solid-state detector. The front surface of each of the two MCPs is biased slightly negatively with respect to the housing to repel low-energy (<100 eV) secondary electrons. A physical partition between the two MCPs prevents secondary electrons of one MCP triggering the other. From *Gloeckler et al.* [1992].

Analyzers – Carbon Foils

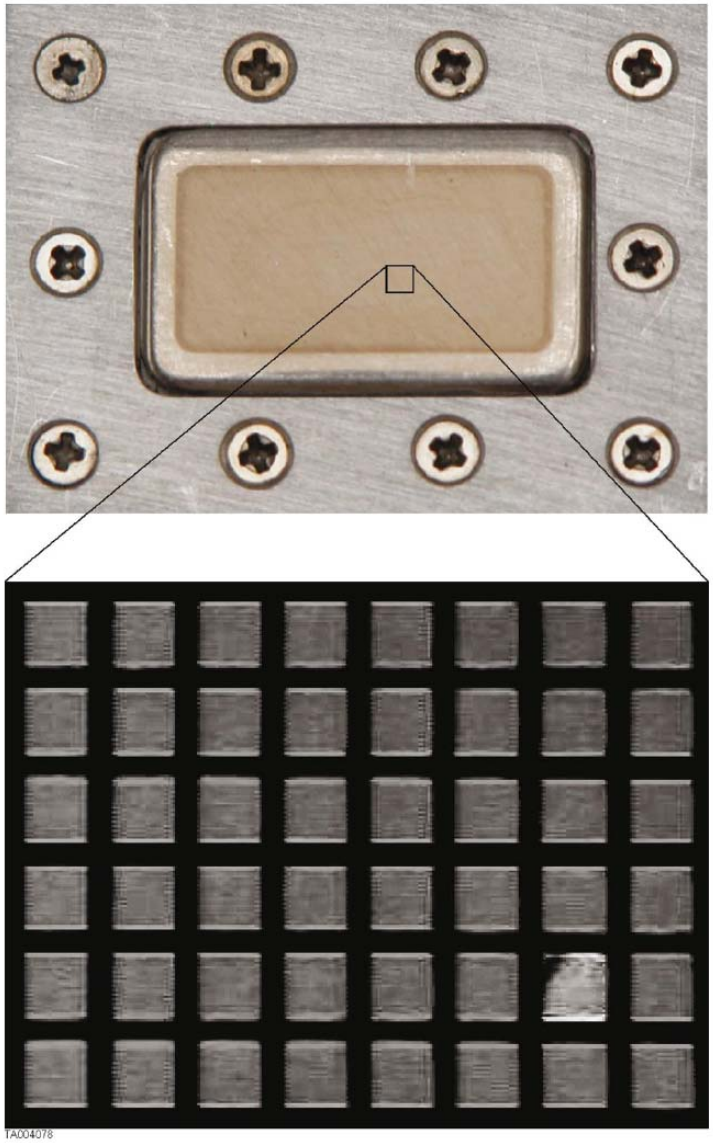

McComas *et al.*

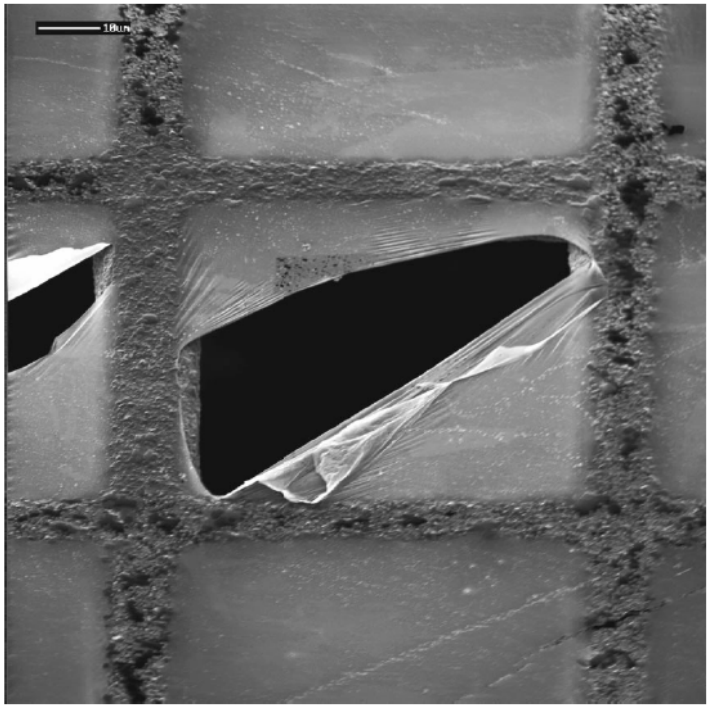

FIG. 1. Secondary electron image of a nominal 0.5 μg/cm^2 foil on a 200 lpi nickel grid using a Ga^+ FIB. The tear was intentionally caused by extremely high fluence bombardment in a rectangular raster area; the upper-left corner of this FIB raster area can still be seen in the remaining foil. Prior to the tear, the foil had the same appearance as the frame immediately above. Note that even when the foil was forced into failure by extreme ion bombardment, the tear was still confined to the individual pane.

Analyzers – ESA + Time-of-Flight

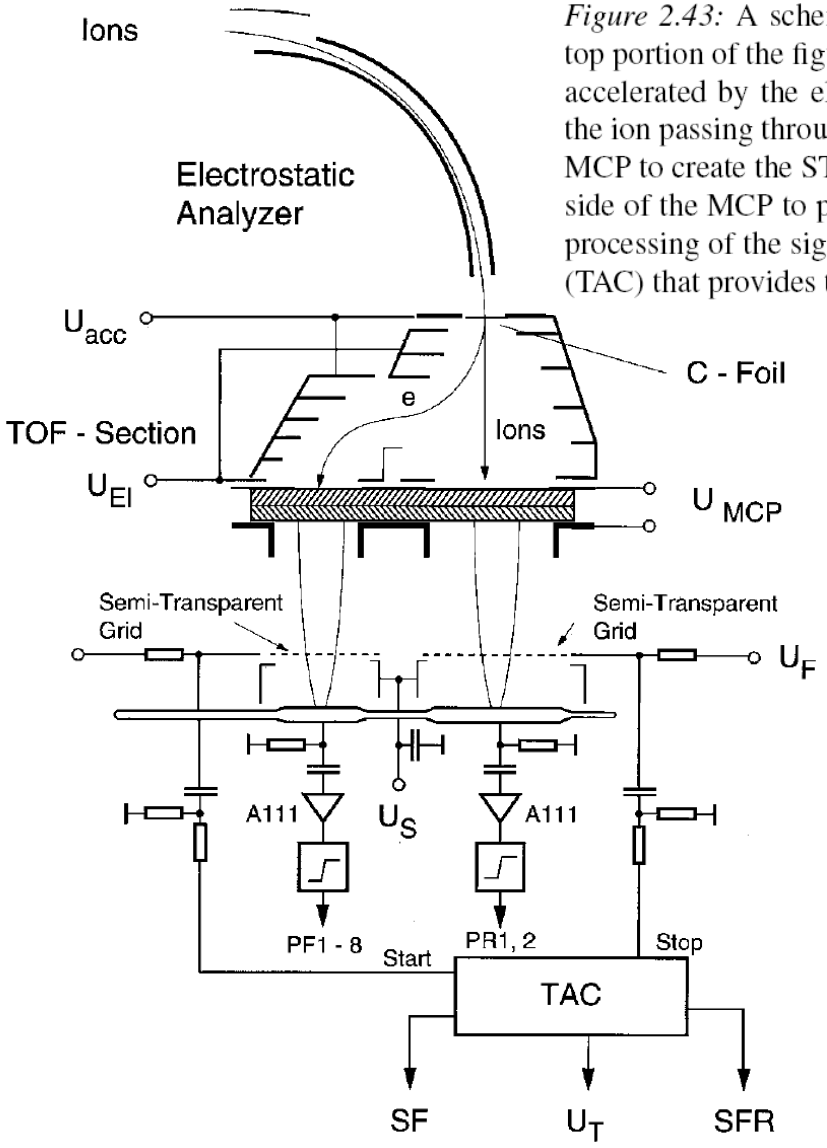

Figure 2.43: A schematic showing the Cluster CODIF TOF principle of operation. The top portion of the figure depicts the motion of an ion through an electrostatic analyzer and accelerated by the electrically biased carbon foil. The secondary electrons produced by the ion passing through the foil are steered by biased electrodes to the left hand side of the MCP to create the START signal while the ion continues on a linear path to the right hand side of the MCP to produce the STOP signal. The bottom portion of the figure shows the processing of the signals from each side of the MCP to the Time-to-Amplitude Converter (TAC) that provides the measure of the time-of-flight of the ion. From *Rème et al.* [1997].

TOF techniques have been combined with ESAs to measure composition. Ions are post-accelerated to >15 keV in order to penetrate the thin carbon foils.

Analyzers – Energetic Neutral

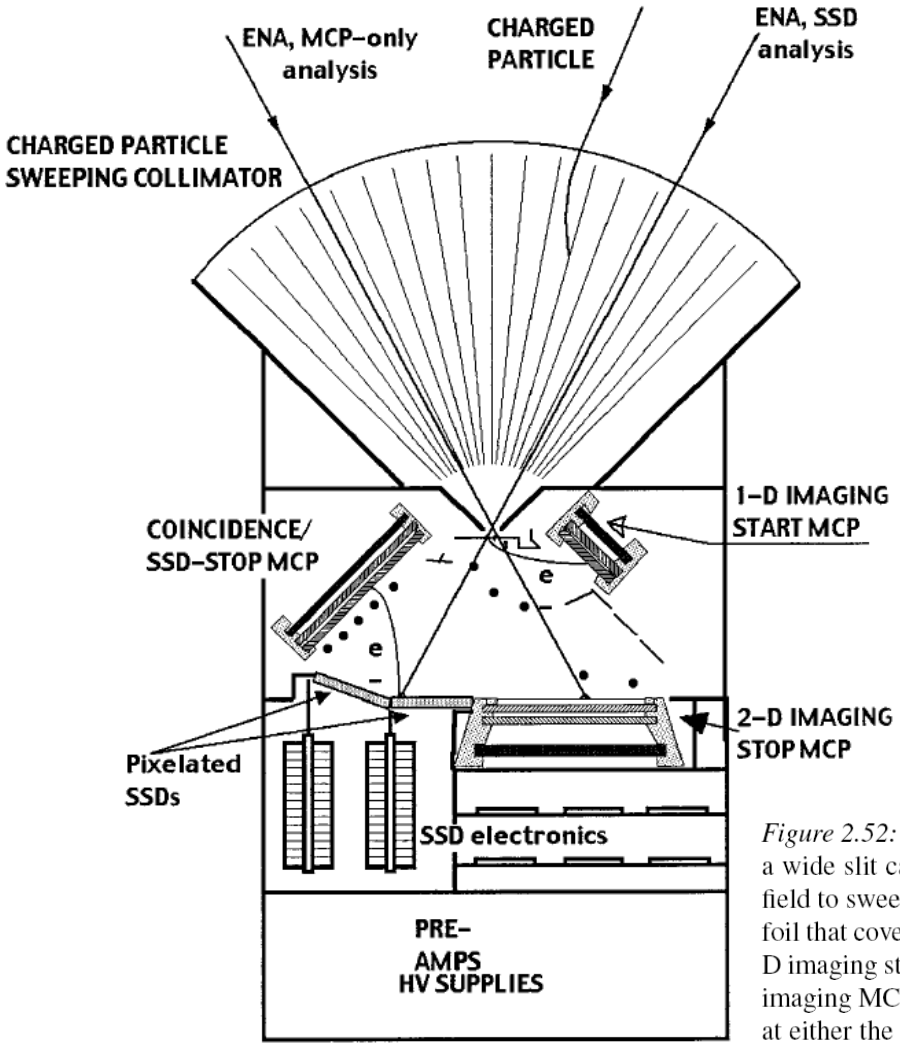

TOF techniques can be combined with electrostatic rejection and solid state detectors to determine energy and composition of energetic neutrals.

Figure 2.52: Schematic drawing of the HENA sensor on the IMAGE spacecraft. HENA is a wide slit camera. Electrically-biased and serrated collimator plates provide the electric field to sweep charged particles out of the entrance slit. Those ENAs penetrating the front foil that covers the entrance slit, produce secondary electrons from the foil to trigger the 1-D imaging start MCP. The same ENAs travel to either the SSD or the back foil and the 2-D imaging MCP immediately behind it. Secondary electrons produced by the arriving ENAs at either the SSD or the front of the back foil are steered to trigger the coincidence/SSD-stop MCP. The dots indicate the locations of the wire electrodes for steering the secondary electrons to their respective MCPs. The spacecraft spin vector is perpendicular to plane of the figure. From *Mitchell et al.* [2000].

Design - Requirements

Start with a science question or motivation:

What causes the aurora?

Science requirements needed to answer the question:

Measure precipitating electrons and ions

Measurement cadence and mission duration

Measurement location (~6000 km, >60^{o} Latitude)

Measurement requirements (depends on satellite/orbit):

Instrument field-of-view.

Anglular resolution.

Energy range and energy resolution.

Sensitivity or geometic factor.

Design - Requirements

Instrument requirements:

- **Analyzer geometry determines energy/angle resolution.**
- **Size of analyzer determines sensitivity.**
- **Detector/Electronics counting rates**
- **Mass and Power**
- **Telemetry rate to get data to the ground.**
- **Housekeeping diagnostics**

Mission requirements:

- **Spacecraft transmitter power**
- **Ground receiver diameter**
- **Solar array size**
- **Fuel/Stationkeeping requirements**
- **Attitude/Orbit/Spin-rate Control/Knowledge**
- **Cleanliness.**

Design – Example Parameters

Requirement	Design Parameter
Energy-Angle resolution	ΔR/R, Anode size
Sensitivity or Geometric Factor	R and ΔR/R
Field of View	Collimation, deflectors
Sunlight Rejection	Blacking ESA
Scattered Particle Rejection	Serrate ESA
Penetrating Background	Anti-coincidence
Uniform response	Machine Tolerance
No HV arcing	Insulator Length
No Out-gassing	Material Selection
Minimum Radiation Shielding	Material Thickness
Survive Vibration	Structural Ribs
Ease of assembly/disassembly	# of screws
Contamination Control	Aperture Mechanism
Long Life	Ground N_2 Purge
Radiation Tolerance	Parts selection
Mass Constraints	Size, material selection
Power Constraints	Electronics Speed
Thermal Constraints	Flexible, Fit tolerance

Design – Example Procedure

1. **Start with a concept (combination of analyzers/detectors/electronics)**
2. **Work out a rough mechanical design based on general knowledge.**
3. **Perform a sanity check with ME/EE (mechanical, optics, electronics)**
4. **Perform simulations to refine the optics (2-D and 3-D)**
5. **Develop preliminary mechanical design – determine limits to optics, subassemblies.**
6. **Perform mechanical sanity check (any exposed insulators, alignment tolerance, vibration issues, ease of assembly)**
7. **Work out a preliminary electrical design – EE sanity check.**
8. **Compare with other techniques (is it simpler?, less resources?, time to start over?)**
9. **Re-run simulations with mechanical design limitations.**
10. **Perform electrical-mechanical interface design (ease of assembly)**
11. **Finish mechanical design (simplify, look for off-the-shelf parts).**
12. **Electronics board layout and parts select, parts qualification (radiation testing)**
13. **Fabricate mechanical prototype and electronics boards.**
14. **Test subassemblies.**
15. **Construct prototype and test for unanticipated problems.**
16. **Re-design and modify to solve unanticipated problems and simplify construction.**
17. **Vibration and thermal vacuum testing**

Design – Common Problems

1. Allowing the engineers to control the design
2. Galling
3. Solder bridge or unsoldered part
4. Ground loops – electronic noise
5. Improper part loading – impossible to read component values.
6. Insulators exposed and charging
7. Tantalum Capacitors loaded backward
8. Improper mechanical fit tolerance for thermal expansion
9. Wrong heat treatment of parts.
10. Incorrect material thickness or clamping for vibration tests
11. Improper load on power supplies when testing
12. Electronic noise – inadequate capacitance on power lines
13. Digital timing problemsLatch up
14. Initialization and power on reset
15. High voltage disable
16. Leakage electric fields through grids
17. Poor baffling for pump out
18. Electronic part latch up

Design – Simulation Tools

1. **Program for calculating electric/magnetic fields with specified boundary conditions**

2. **Ray tracing program – with plot routines**

3. **Analyzer characterization routine – (finds the space of throughput trajectories)**

4. **Plotting routines for analyzing response.**

5. **Routines for calculating particle transmission through materials (Casino, SRIM/TRIM)**

6. **CAD program for mechanical drawings**

There are commercial programs available
Or you can write your own program in day or two.
Optimized programs could take a couple of weeks to write.

Design – Simulations

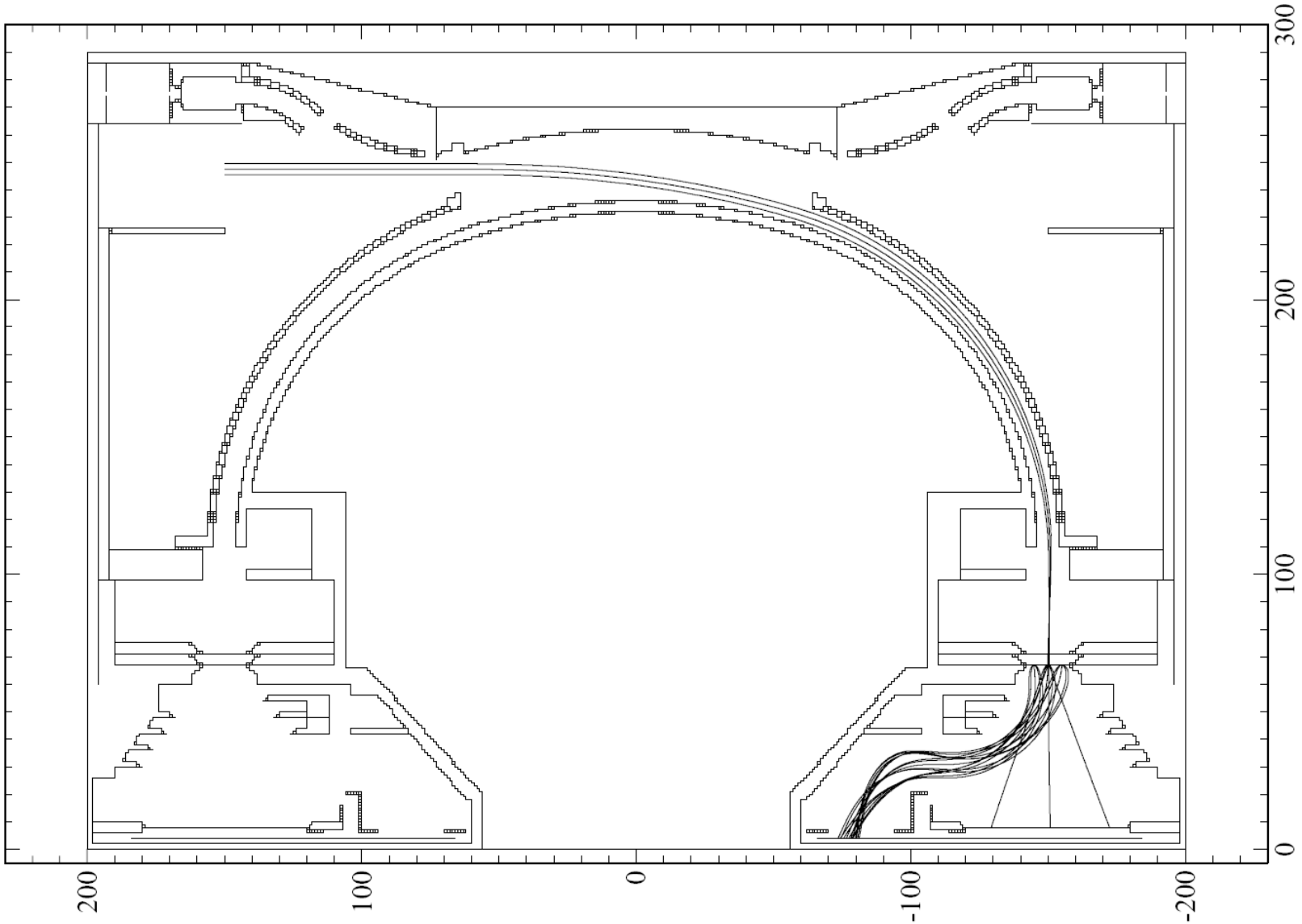

Design – Simulations - Focusing

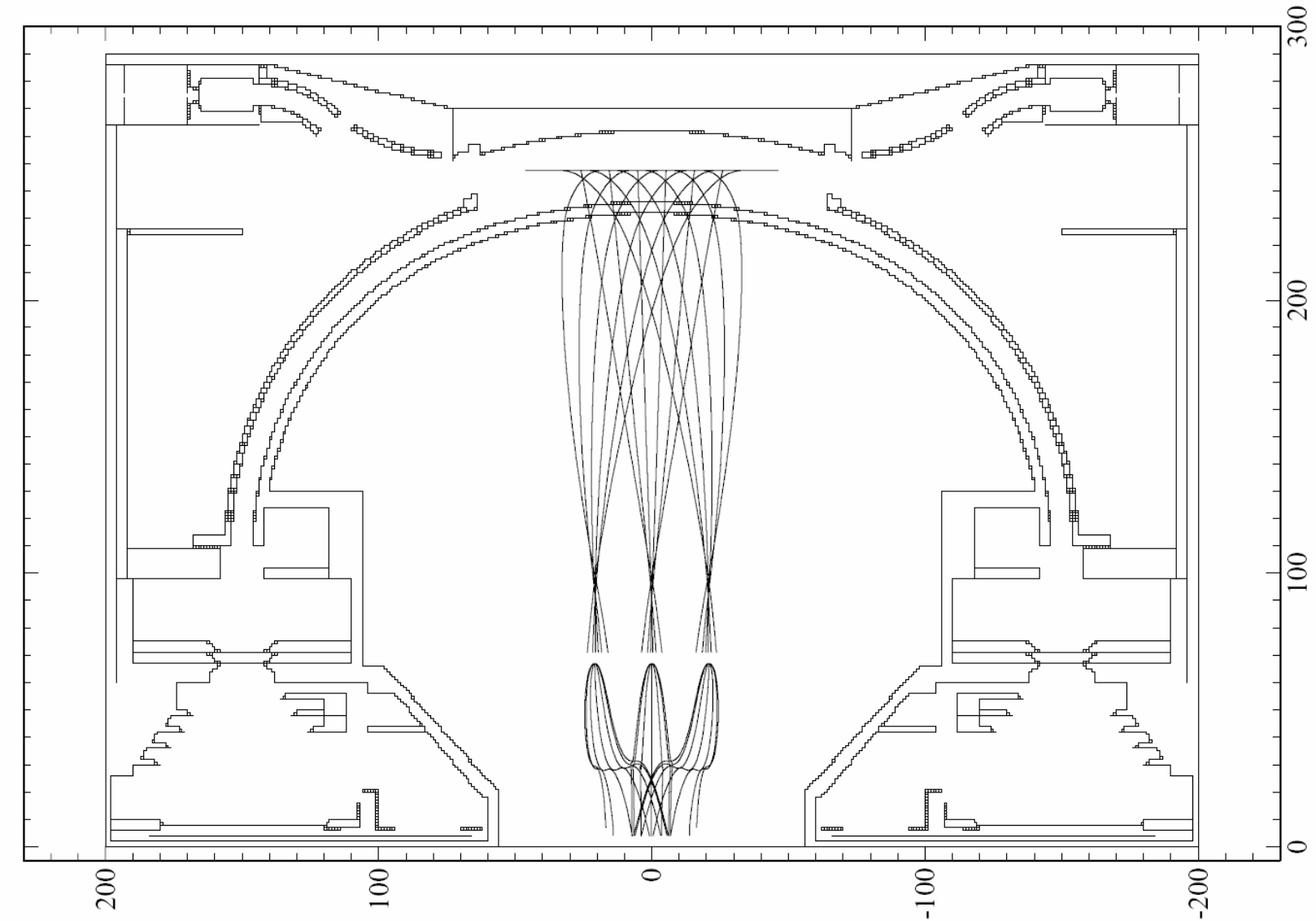

Design – Simulations – Optimize Throughput

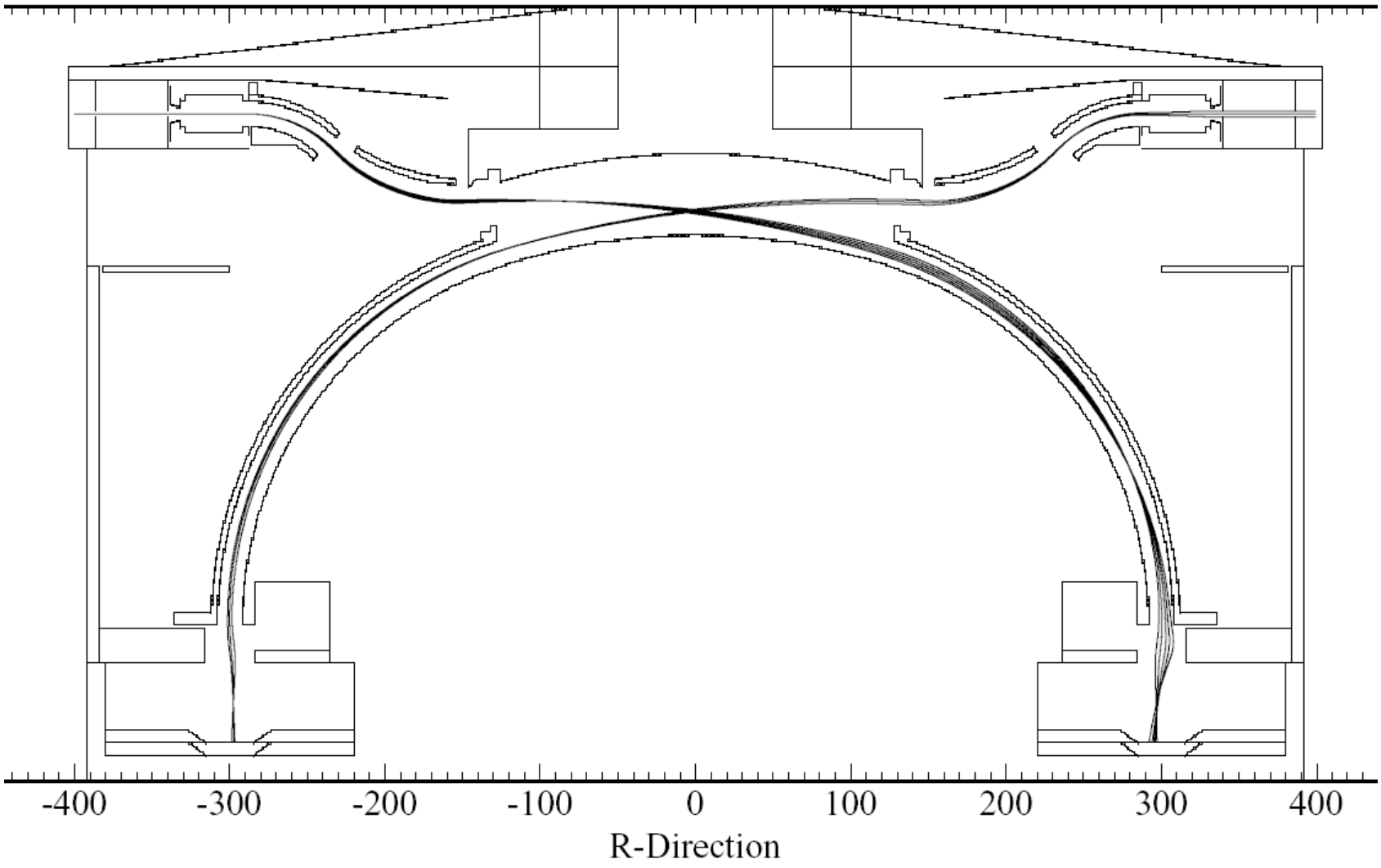

Design – Energy/Angle Response

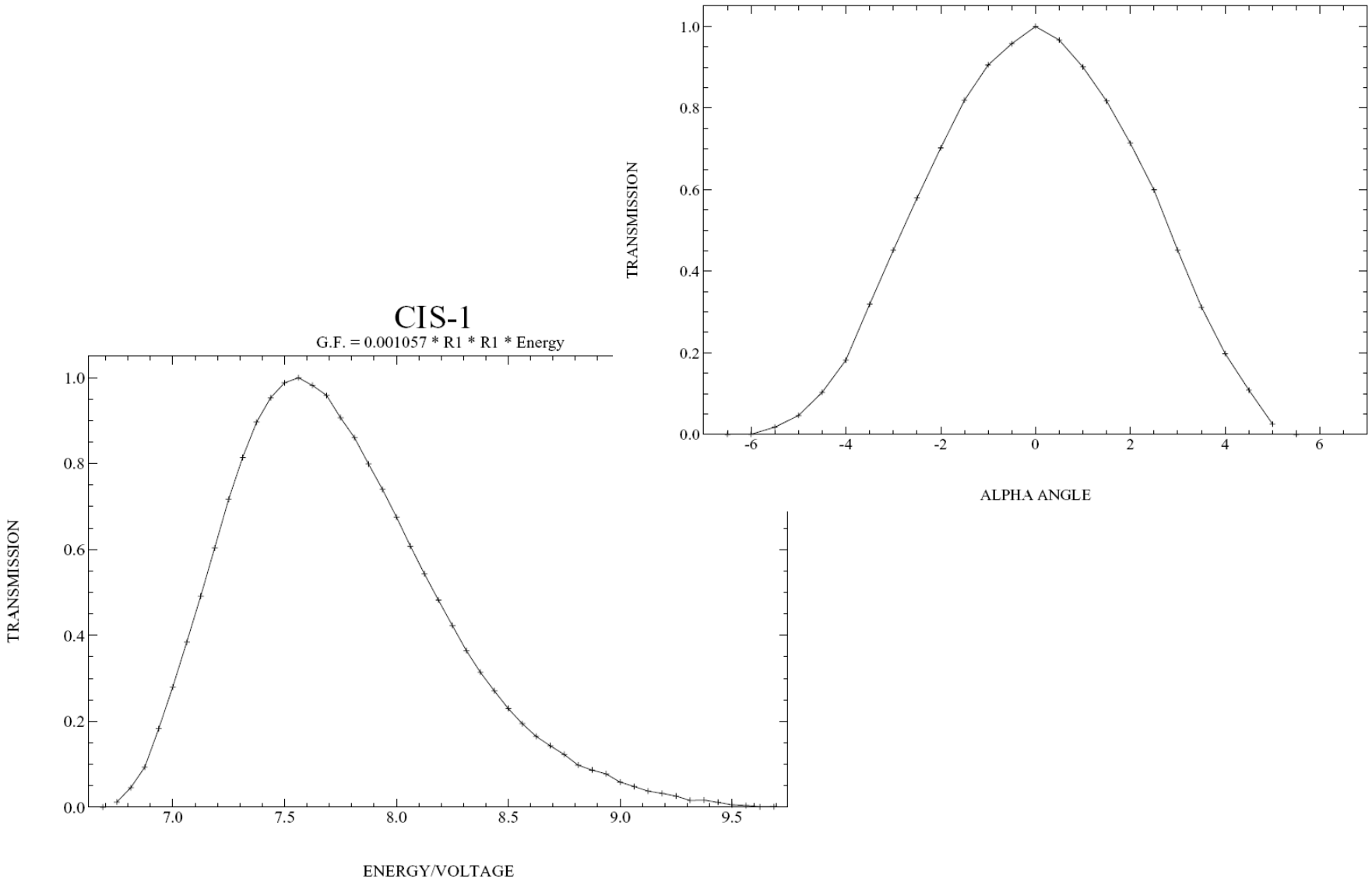

Design – Simplify, Modularize

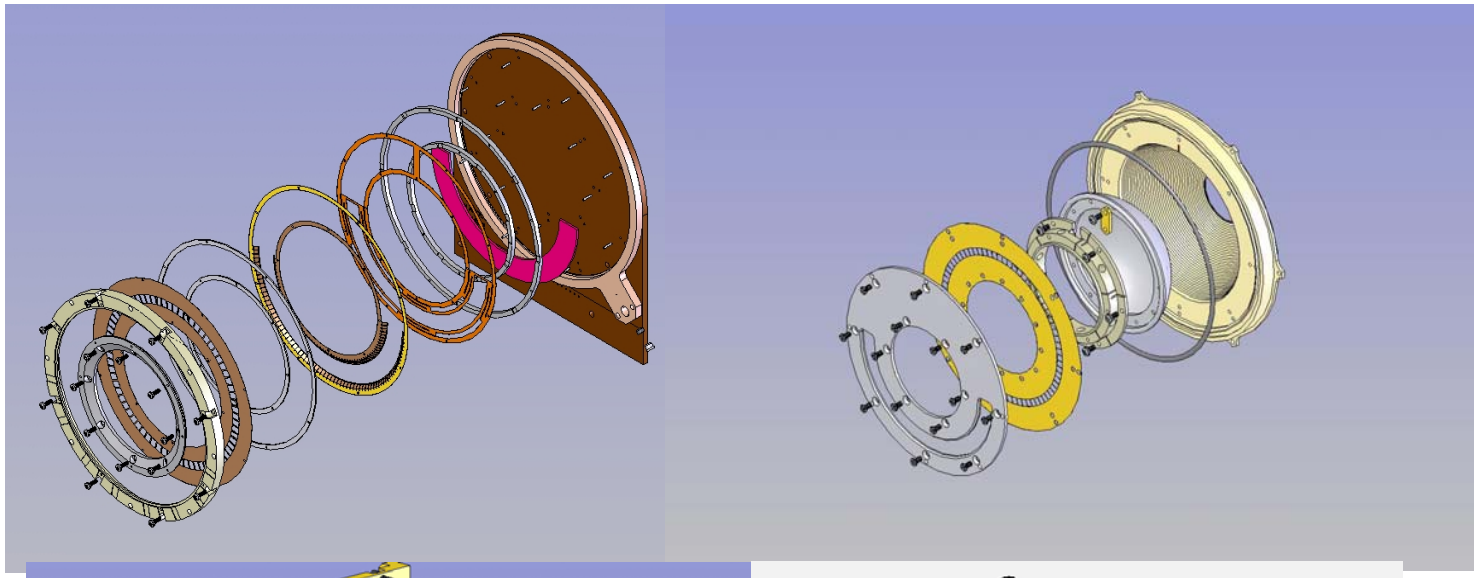

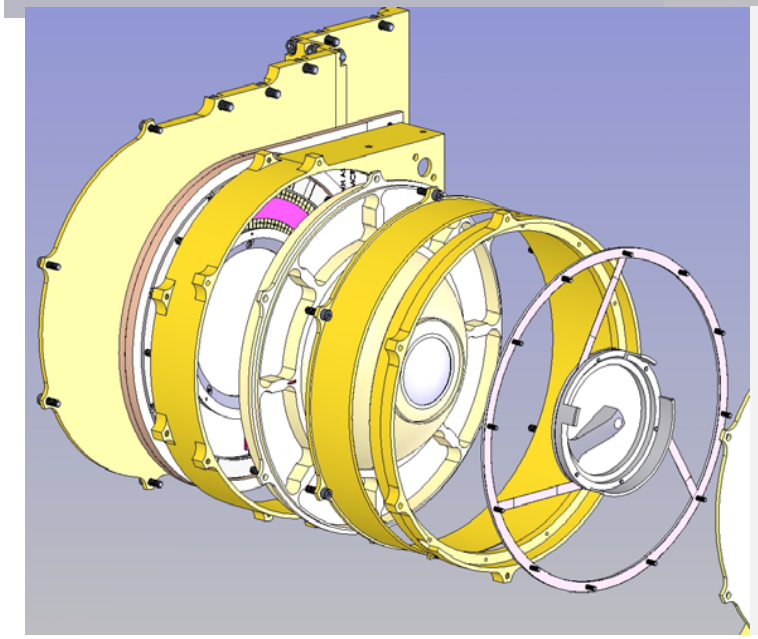

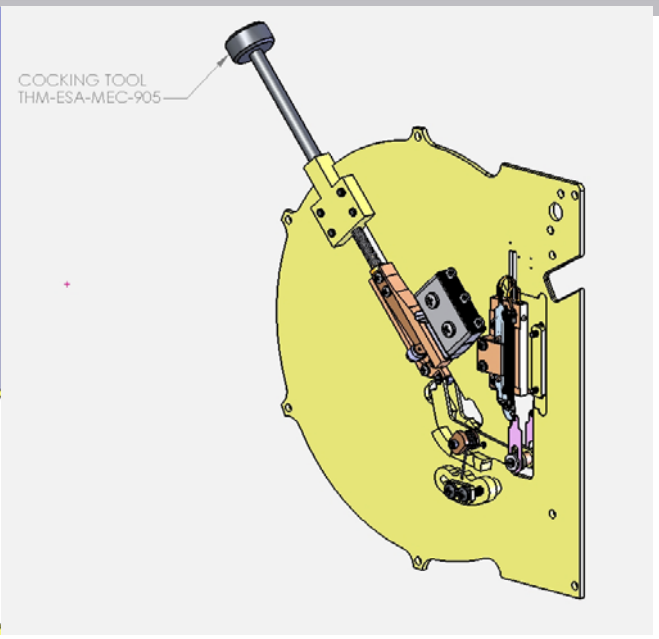

Design – Modular Electronics

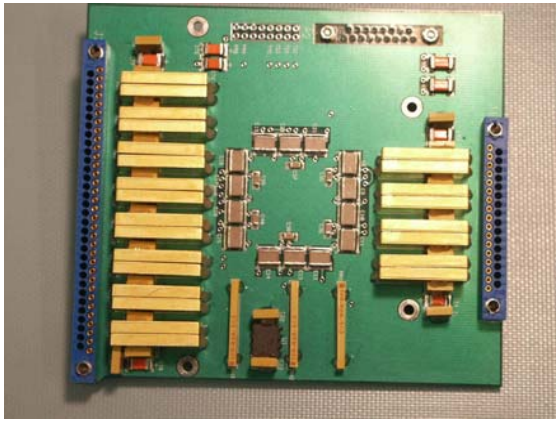

Preamplifier –Front

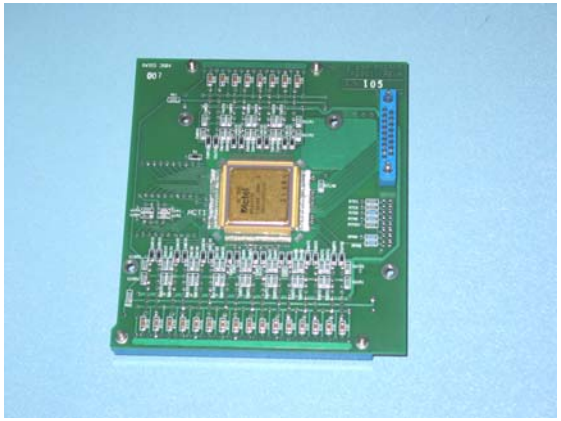

Preamplifier-Back

Low Voltage Power Supply

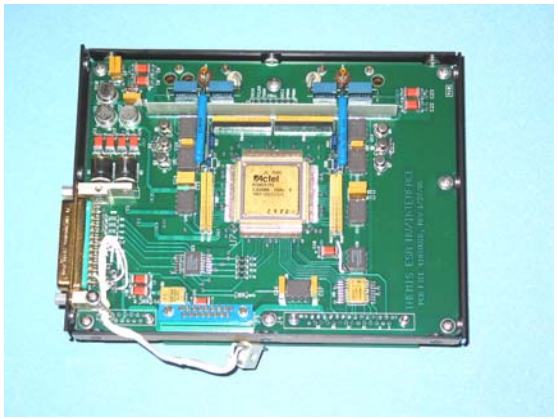

Interface/HVCtrl –Front

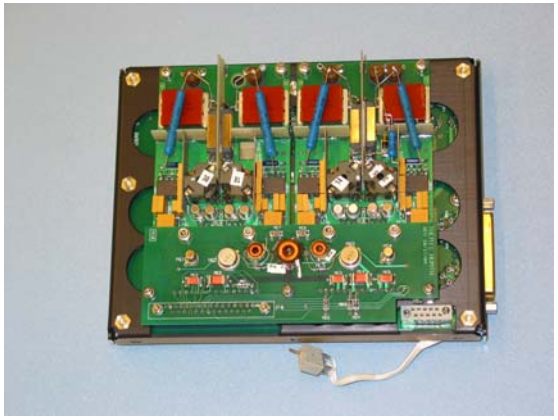

Interface/HVCtrl-Back

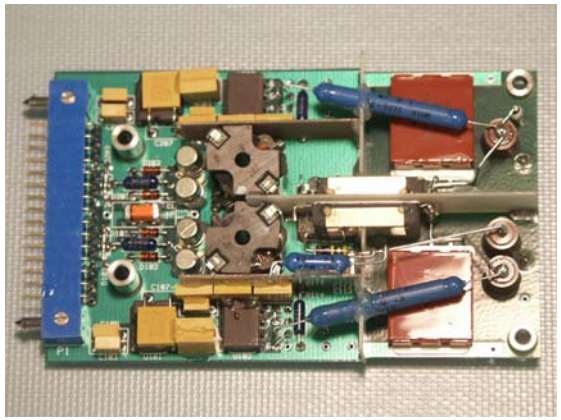

Dual HV Power Supply

Calibration – Procedures

In the old days, instruments were designed by estimating sensor performance based on analytic models.

Ground calibrations were required in order to quantify the instrument's energy and angle response.

Modern instruments can be simulated, and ground calibrations are primarily a check of proper instrument construction.

Calibration curves are generally compared with simulations, providing a functional test of proper operation.

The primary parameter calibrations determine is the energy constant.

Calibration – Tests

Detector characterization – matching MCP pairs

Background tests – looking for hot spots, arcing

Energy constant test – vary beam energy & elevation

Concentricity test – vary energy and rotation angle

Sensitivity Uniformity – slow rotation at peak energy/angle

Energy sweep test – confirm flight operation modes

Thermal vacuum test – operates properly over temp range

Data packet tests – check onboard data compression

Calibration – ESA Top-Hat

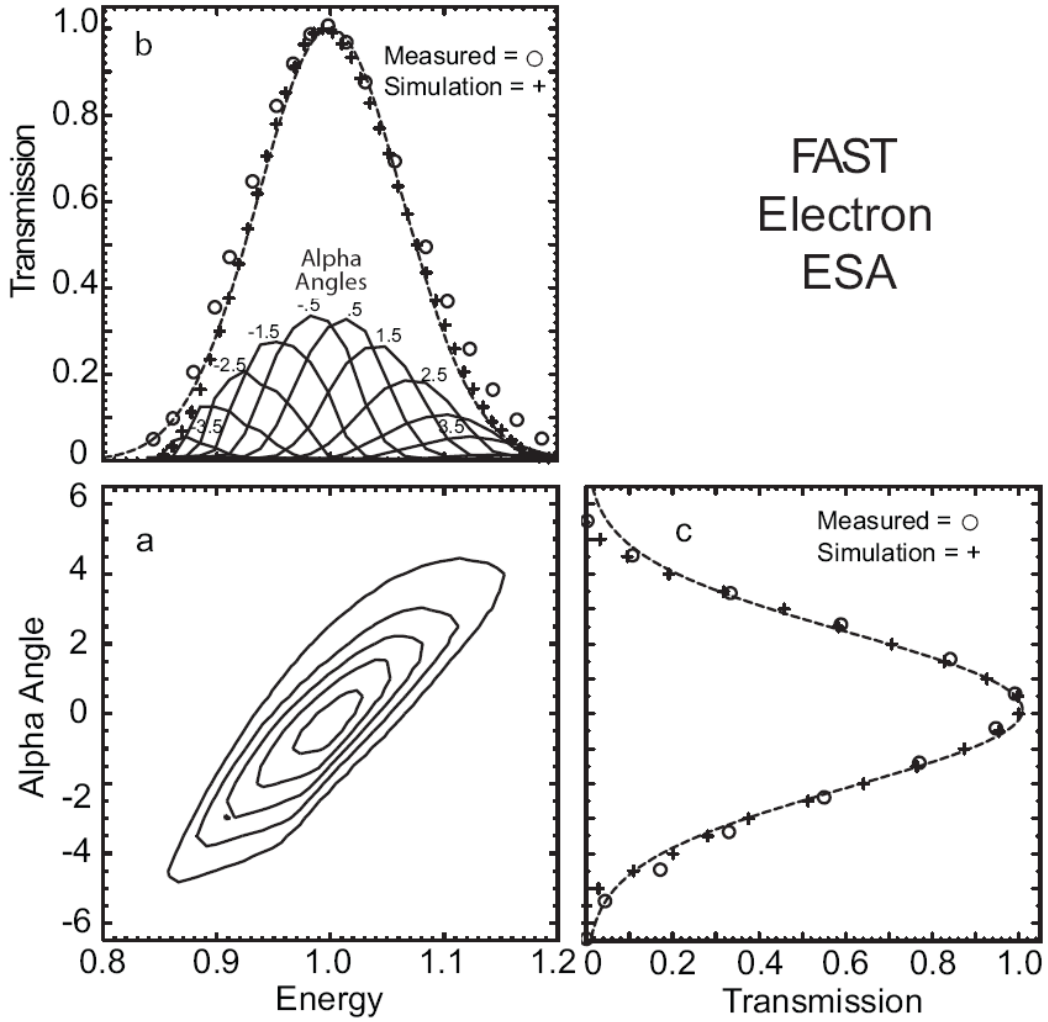

FAST Electron ESA

Comparison of ground calibration data and simulations

Figure 3.6: The input energy and angle response of the FAST electron ESA are compared to numerical simulations and a Gaussian fit. Adapted from *Carlson and McFadden* [1998].

Calibration – Poorly designed

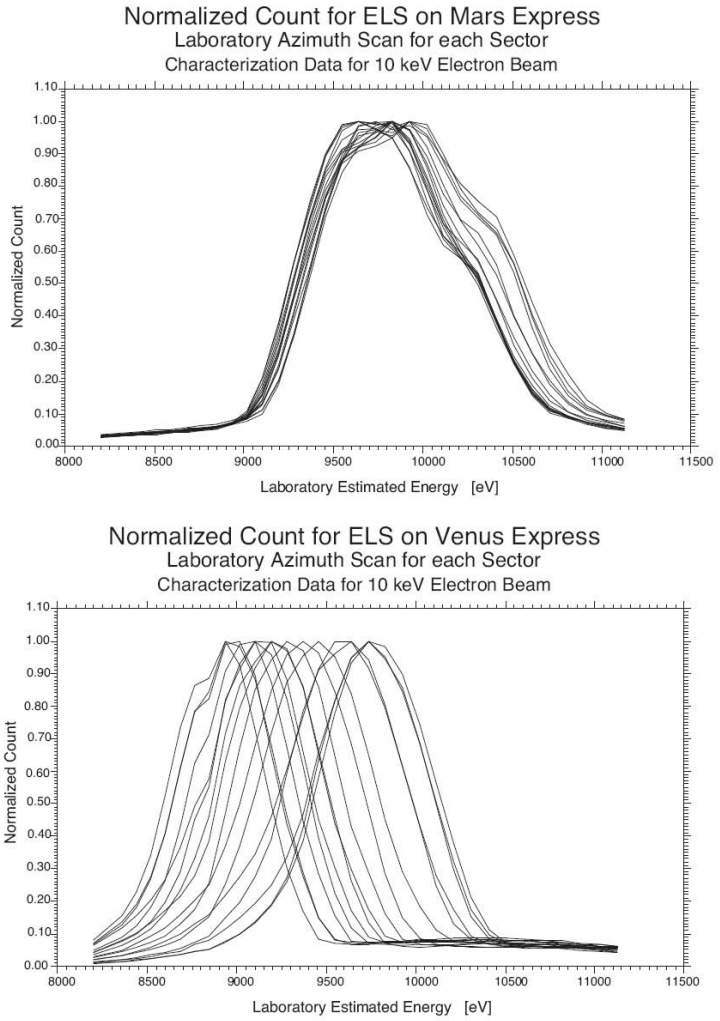

Figure 3.7: Normalized counts of energy scans for the 16 azimuthal sectors of the ASPERA-3/ELS sensor (top), and the ASPERA-4/ELS sensor (bottom), for the European Mars Express and Venus Express missions, respectively. From *Frahm* [2005].

Plots show the energy response at different look direction of two nearly identical instruments.

Non-concentricity of the analyzer hemispheres in the Venus Express sensor (lower plot) produced non-uniform energy response with look direction.

The Mars Express sensor (upper plot) was adjusted by hand to improve its response.

Calibration – Good Symmetry

THEMIS in-flight calibration was facilitated by having sensors with excellent concentricity – typically less than 1% variation in energy with look direction.

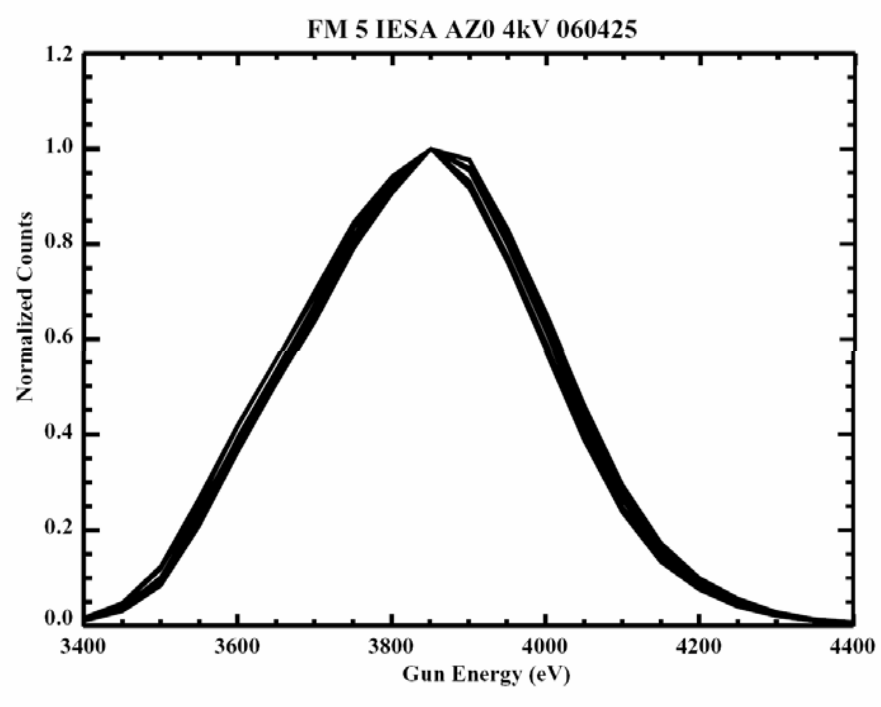

This near perfect concentricity was obtained under normal assembly -- without heroic efforts to align hemispheres.

The mechanical design resulted in alignment determined by a single interface.

Calibration – Uniform Response

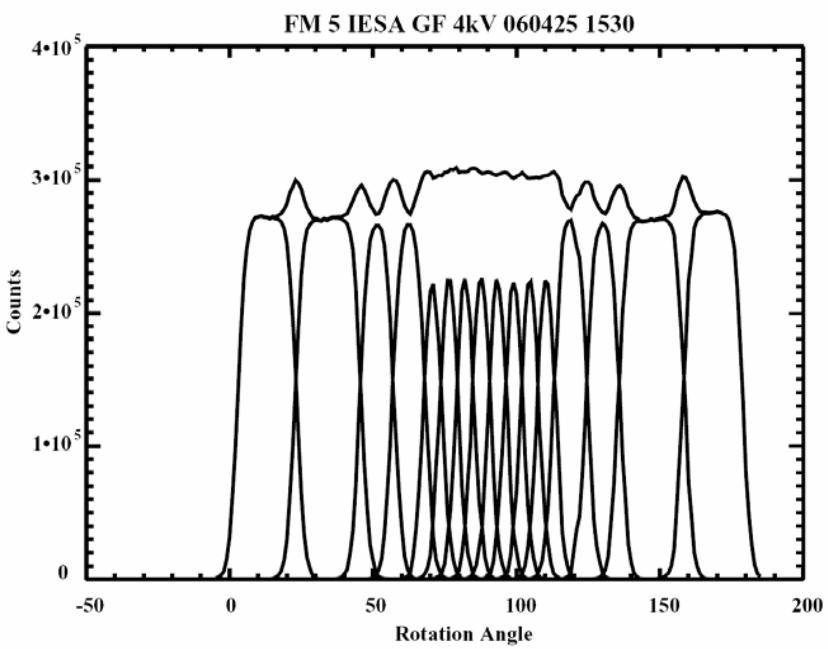

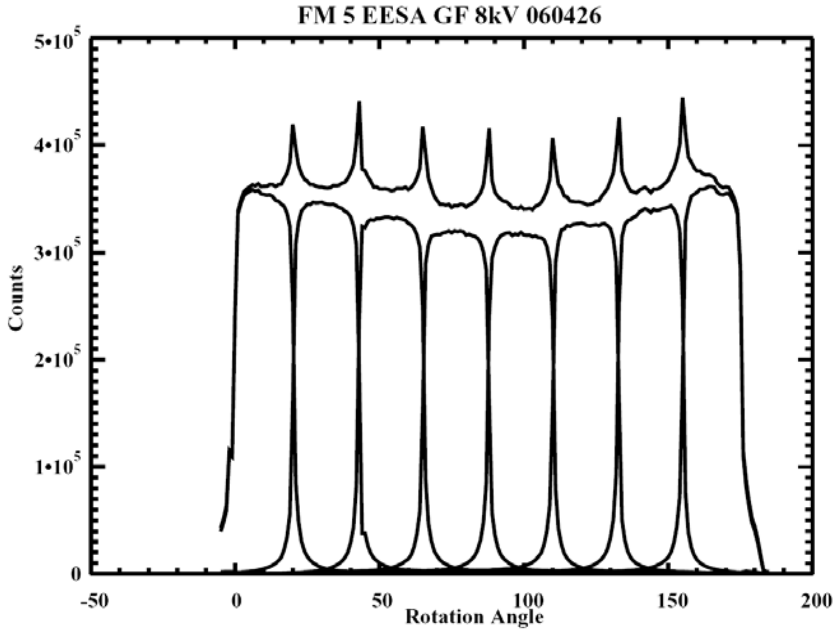

THEMIS ion ESA uniformity test.
Anodes come in 3 sizes – 22.5^{o}, 11.25^{o} and 5.6^{o}.

THEMIS electron ESA uniformity test.
Double counting occurs at borders between anodes.

Calibration – Leakage Fields

Enhanced ion ESA efficiency at low energies is probably due to leakage fields from the MCP through the analyzer exit grid.

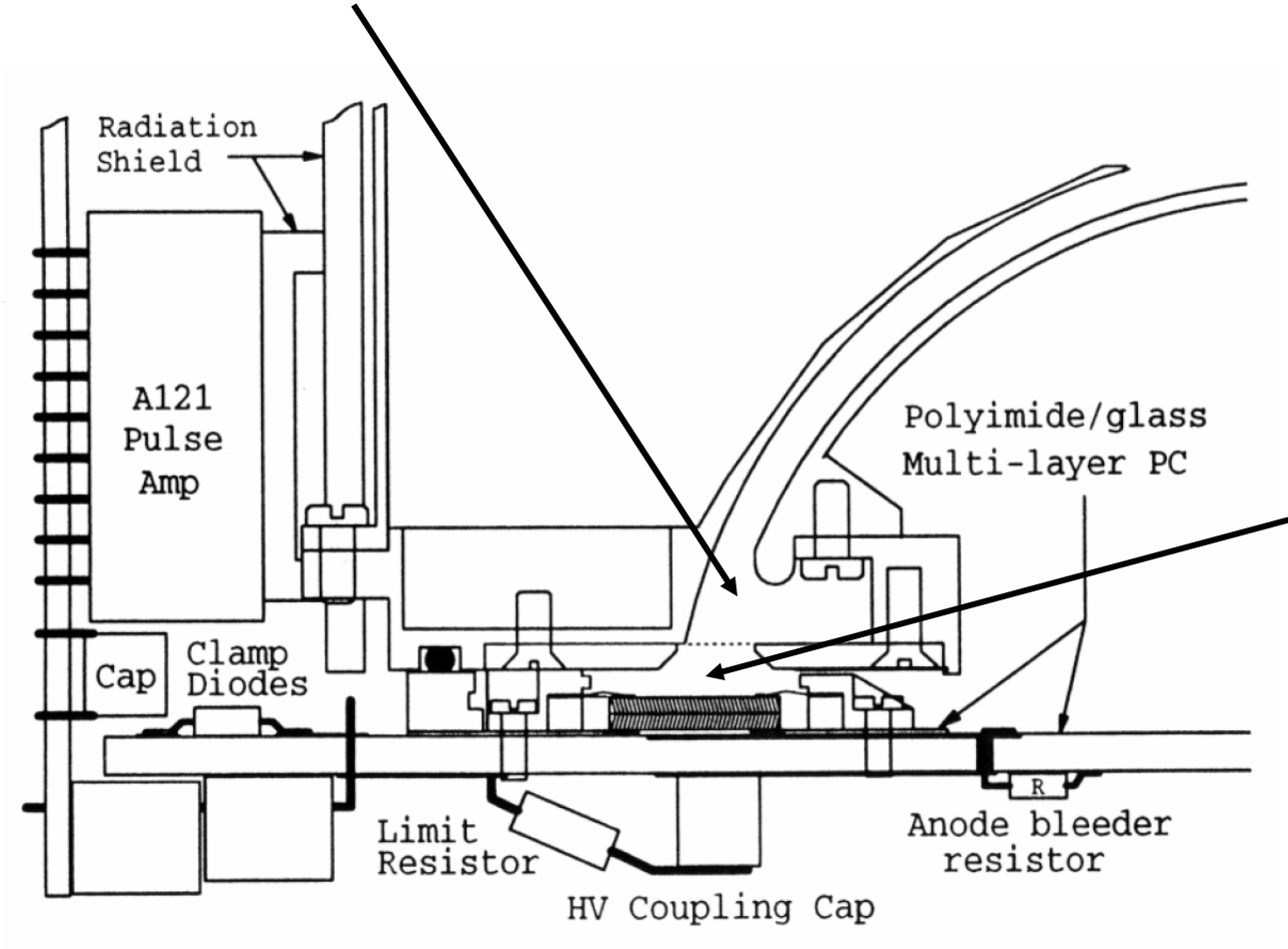

-2 kV on front of MCP

Calibration - Out of Band Response

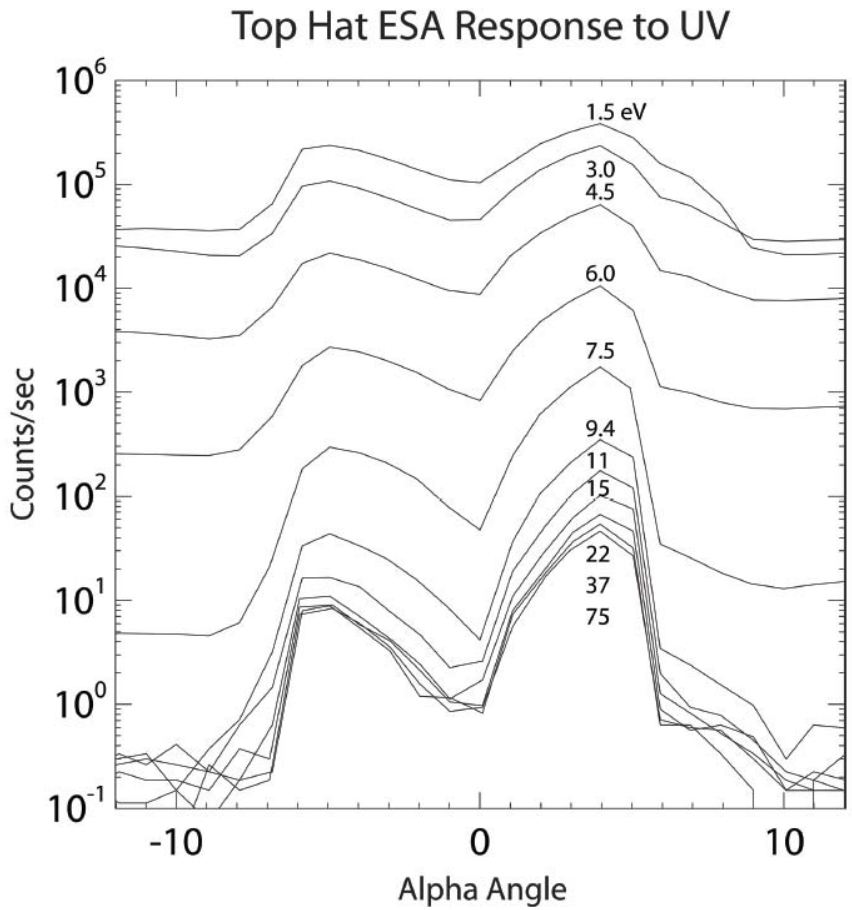

Figure 3.9: Angle response of a top-hat ESA to a Lyman-α photon source. Curves are labeled for values of the analyzer pass energy between 1.5 and 75 eV. The response for energy settings higher than 10 eV is mainly due to scattered photons reaching the MCP. At lower energy settings, photoelectrons produced inside the analyzer dominate over scattered photons. From *Carlson and McFadden* [1998].

Solar UV scattering to the detector can be eliminated with proper blacking (ebanol-C).

Photo-electrons at the aperture are more difficult to eliminate.

Instruments – Wind 3DP

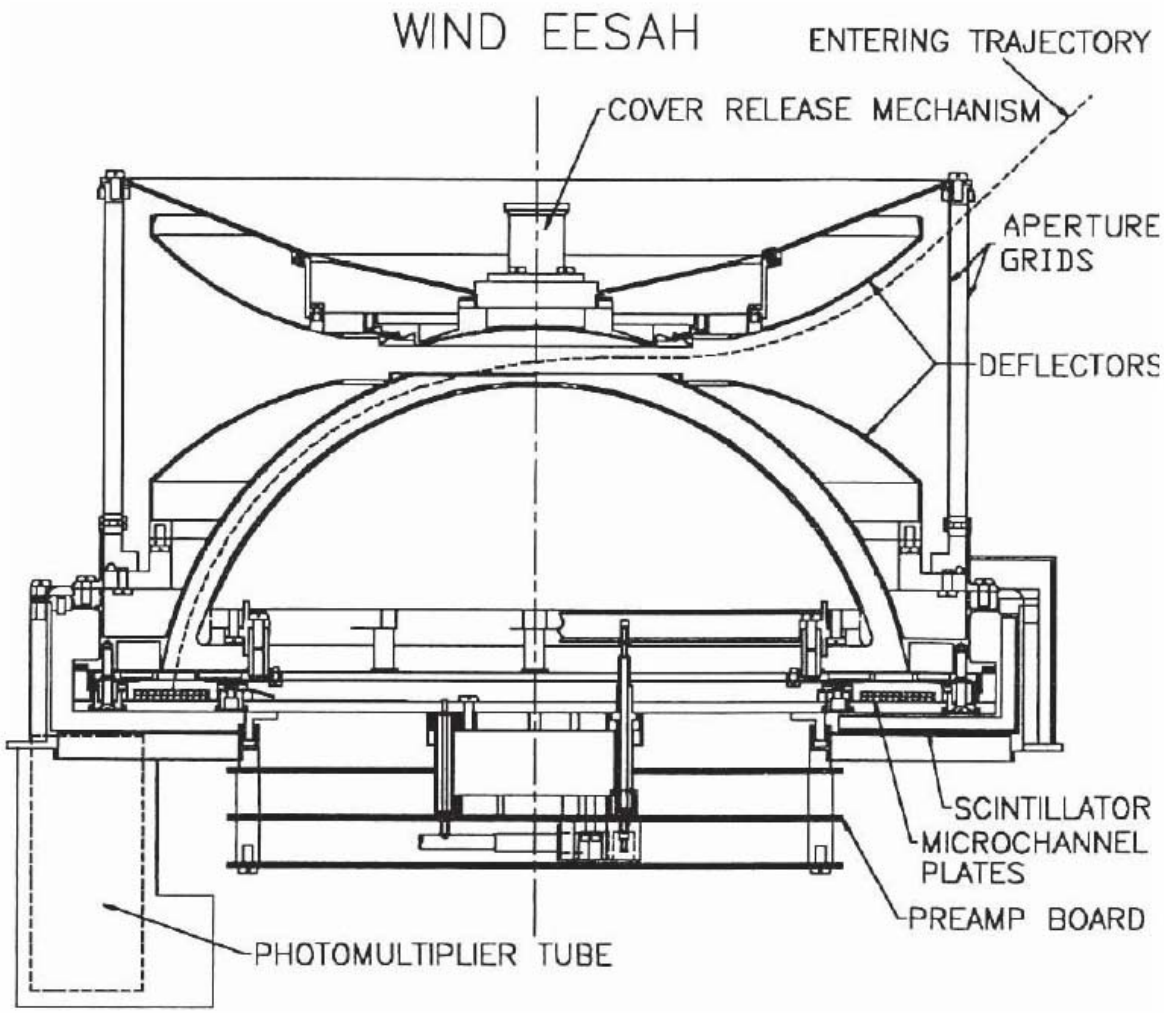

Figure 2.34: Top-hat analyzer EESAH on Wind spacecraft. From *Lin et al.* [1995].

Design included scintillator to reduce background from penetrating radiation

Instruments – THEMIS/FAST

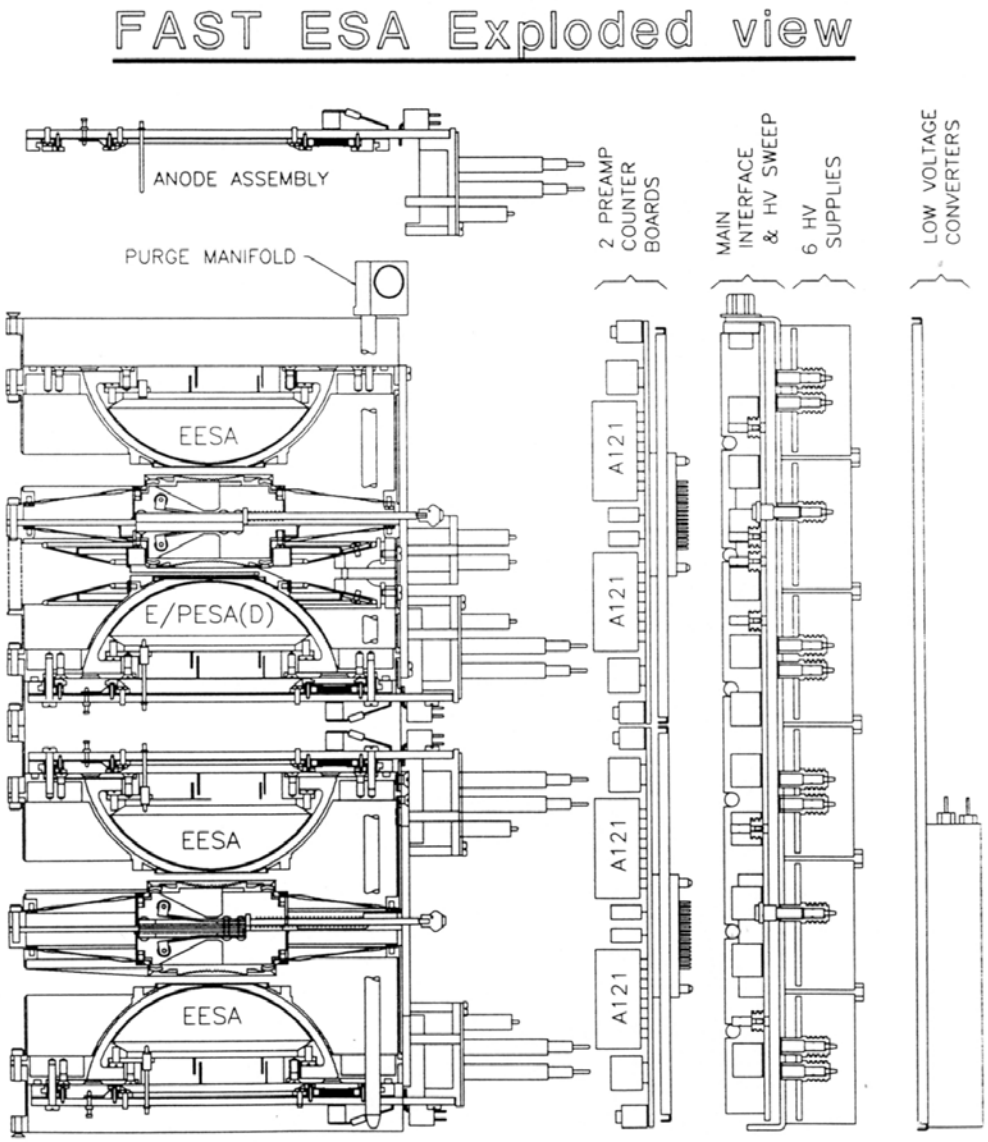

FAST analyzers were designed to be modular.

Subsystems could be easily tested.

Common mechanisms. Common shielding.

Designed for ease of assembly. Few screws.

Contamination control includes aperture closer and purge.

Instruments – Cluster-CODIF

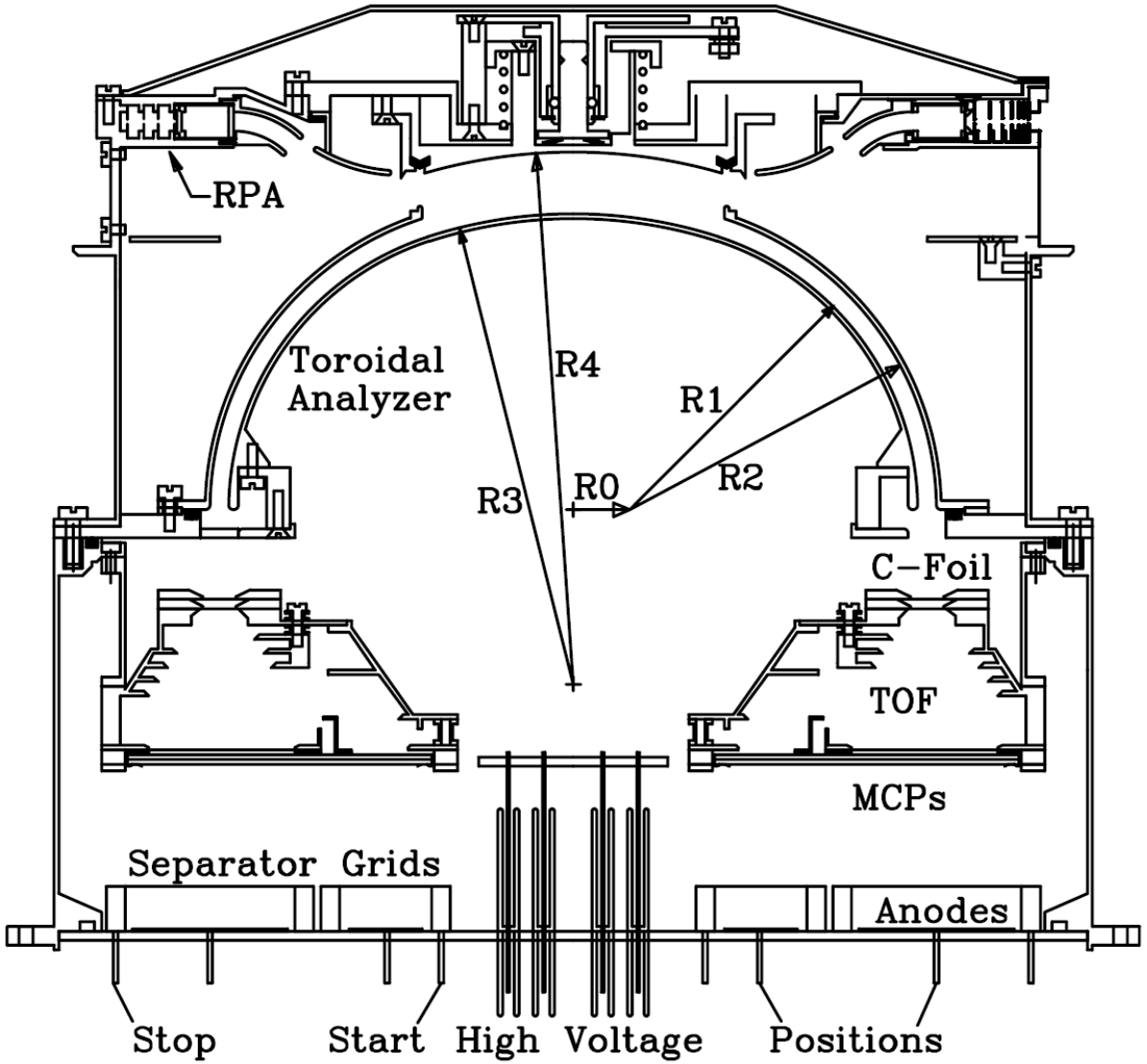

First combined top-hat & TOF

Use of grids & anodes to separate charge for TOF and position imaging

Includes separate aperture for retarding potential analyzer

Instruments - TIMAS

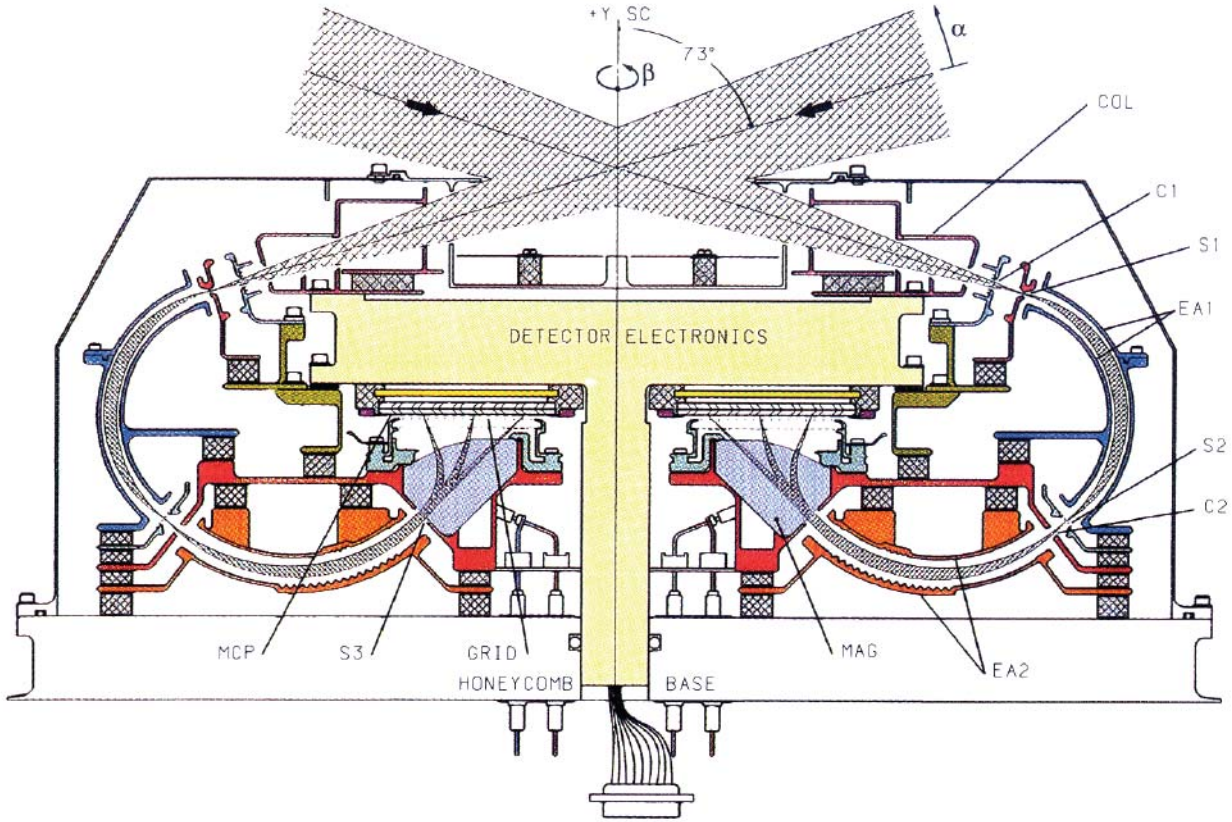

Figure 3.21: Schematic cross section of the TIMAS ion optics. Elements include the collimator, COL, ion repeller, C1, object slit, S1, first toroidal electrostatic analyzer, EA1, image slit for EA1, S2, first field terminator for EA2, C2, second toroidal electrostatic analyzer, EA2, second field terminator for EA2, S3, sector magnets, MAG, grid assembly, GRID, microchannel plate detector, MCP, and detector electronics. The entire assembly is rotationally symmetric about the vertical center line. From *Shelley et al.* [1995].

Complicated double focusing mass spectrometer

No magnet yoke needed

Relatively low sensitivity compared to TOF analyzers.

Instruments – STEREO-PLASTIC

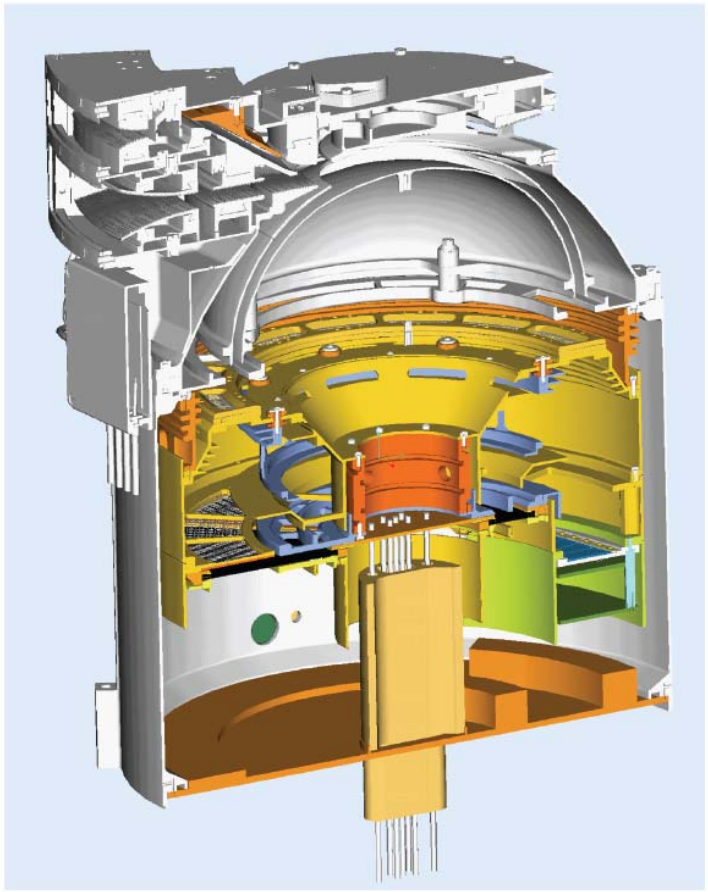

Top-at w/ deflectors

Separate solar wind analyzer entrance

MCPs and SSDs.

Figure 3.24: Cross sectional diagram of the PLASTIC instrument for the STEREO mission [*Galvin et al.*, 2006]. From top to bottom: Entrance system, toroidal electrostatic analyzer, carbon-foil time-of-flight mass spectrometer, MCP and SSD detectors. The electrostatic entrance system, the energy analyzer, and the TOF MS are rotationally symmetric about the vertical center axis (aside from the different geometric factor in solar wind direction pointing to the left).

Instruments – Low Energy Neutral

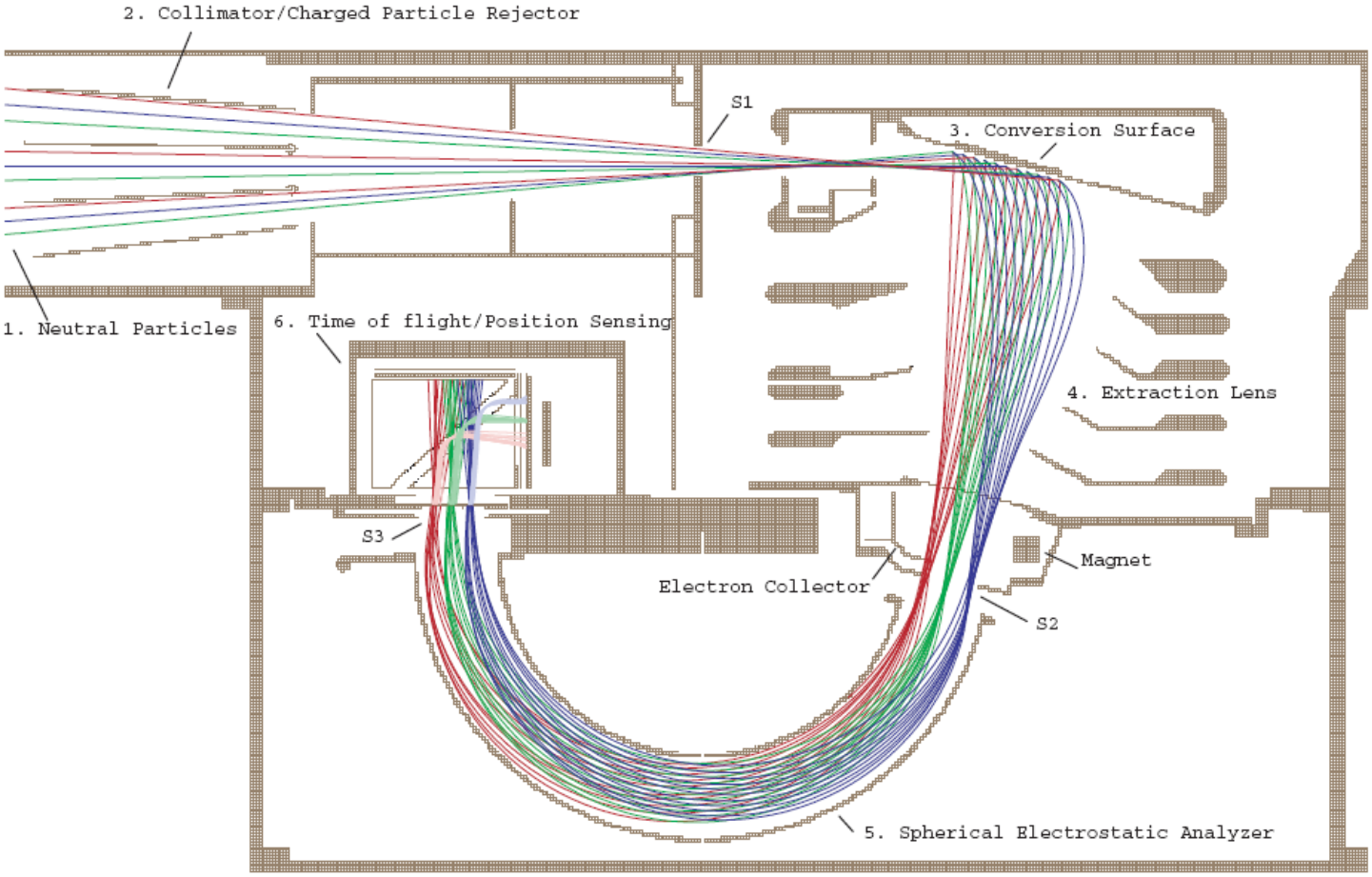

Figure 2.54: End-to-end simulation of the ion optics of LENA, also showing the TOF optics in a 2-D section through the symmetry axis of the instrument. From *Moore et al.* [2000].

Instruments – Sounding Rocket

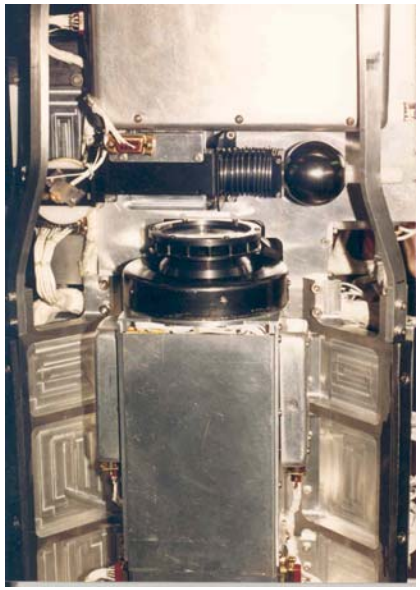

Top-hat ESAs

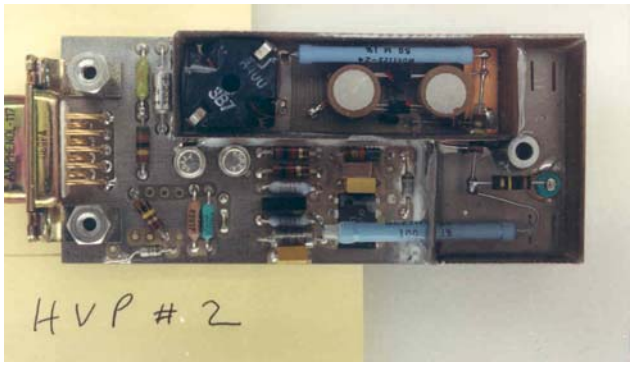

Compact HVPS

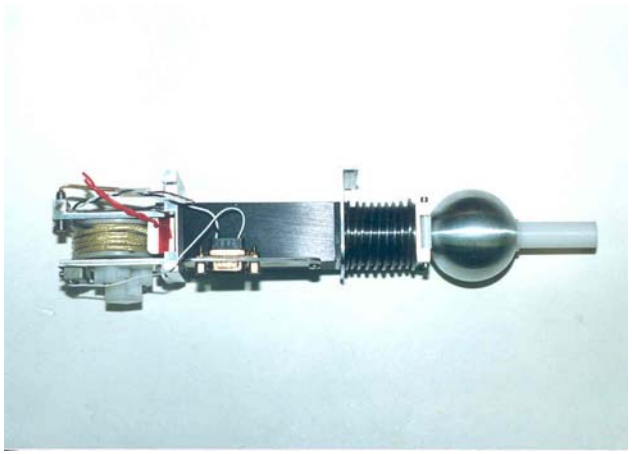

Stacer Booms

Burst Memory

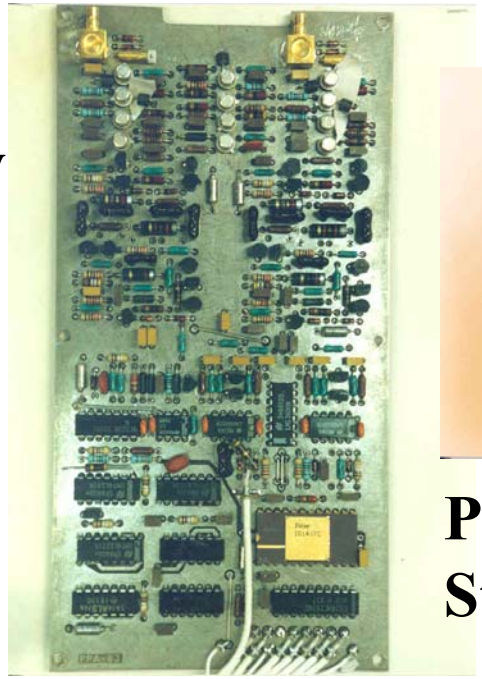

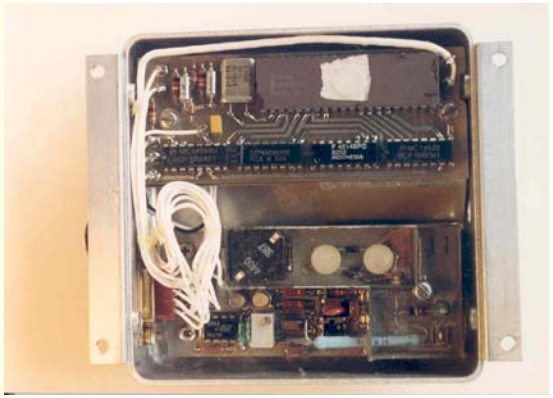

Processor controlled Star Sensor

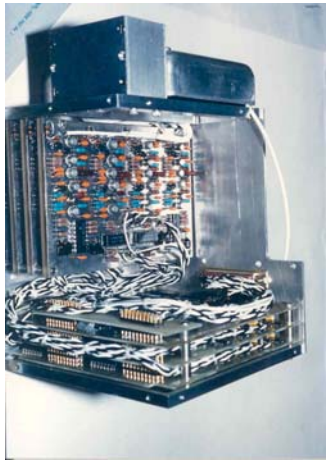

Fast Electron Spectrograph And Wave-particle Correlator

Instruments – Sounding Rocket Payload layout

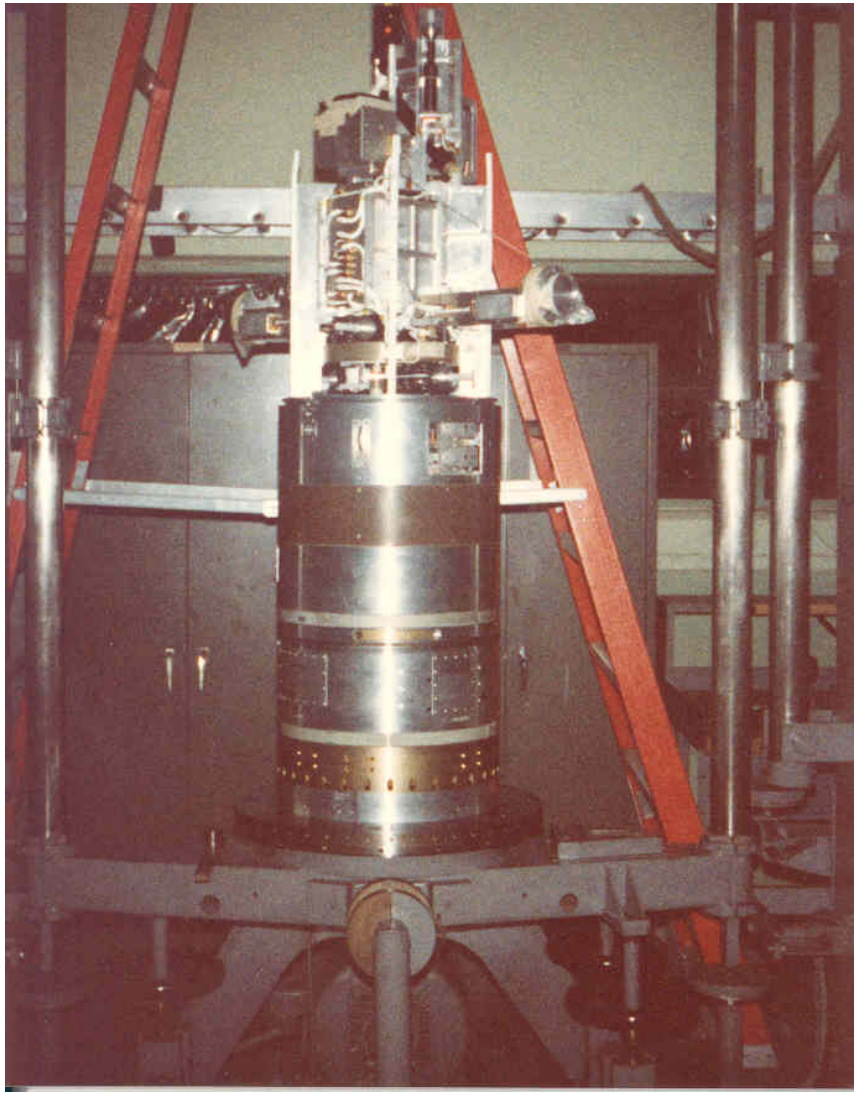

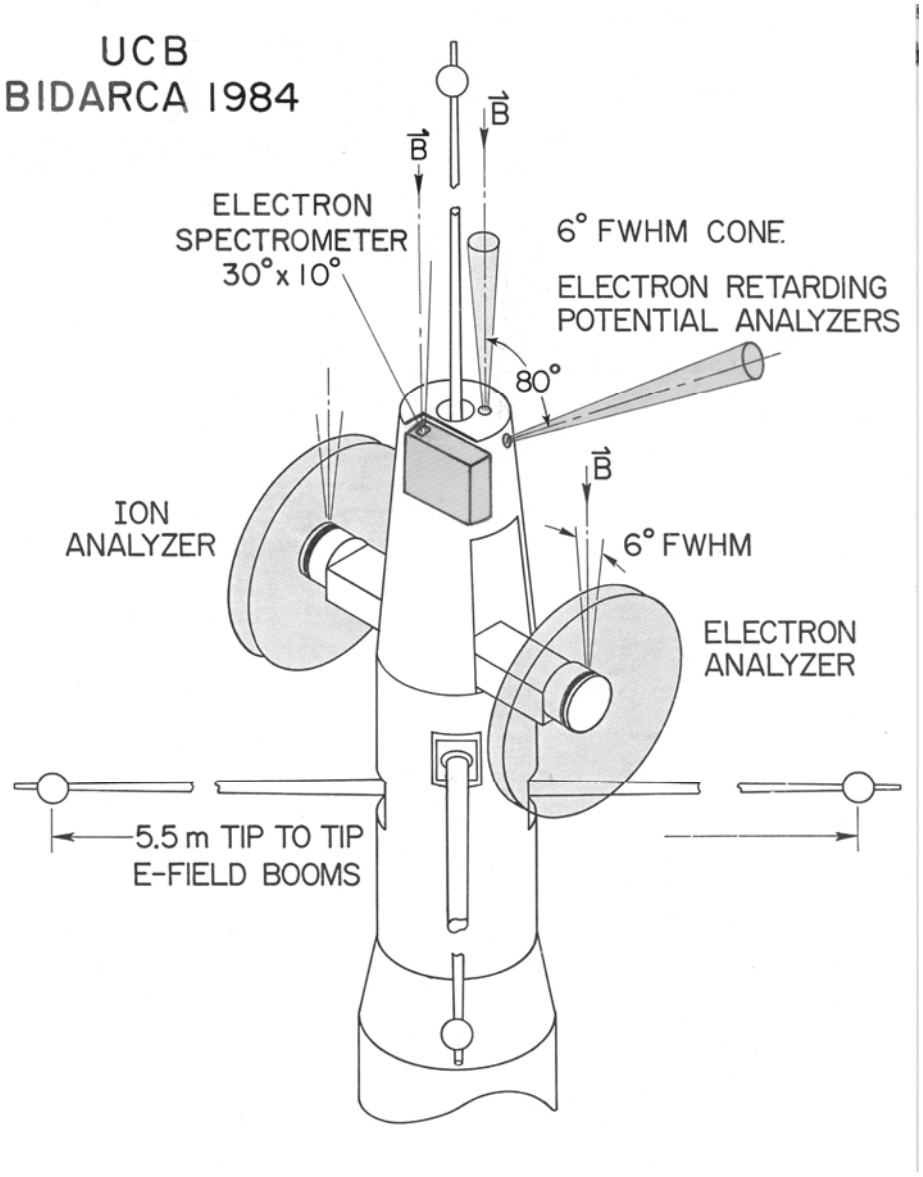

Instruments – Can be part of structure

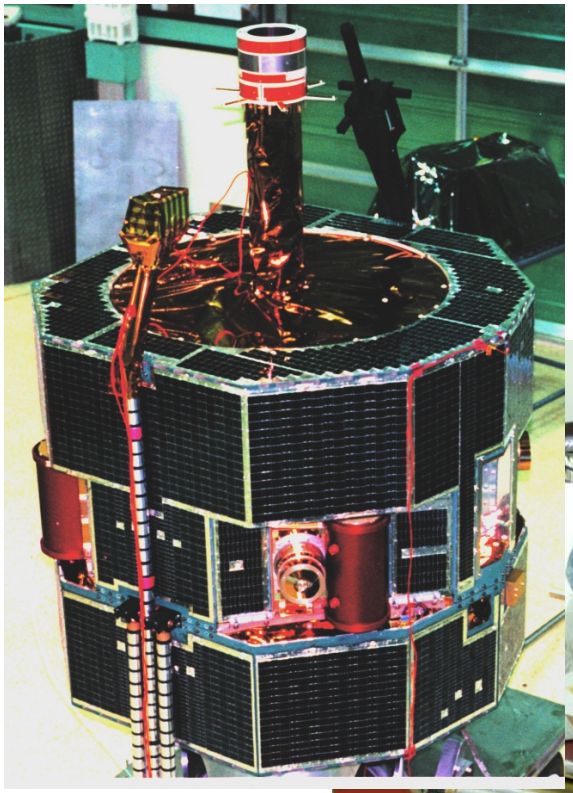

Instruments can provide mech. structure to reduce mass.

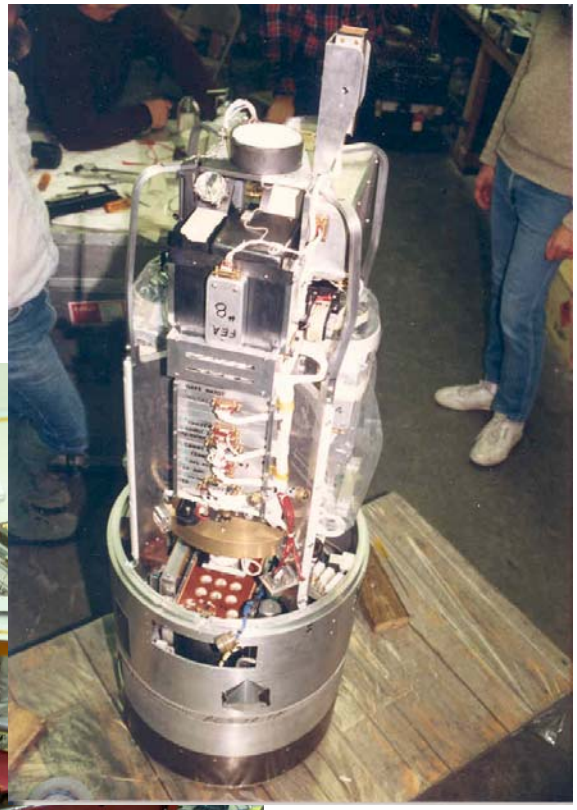

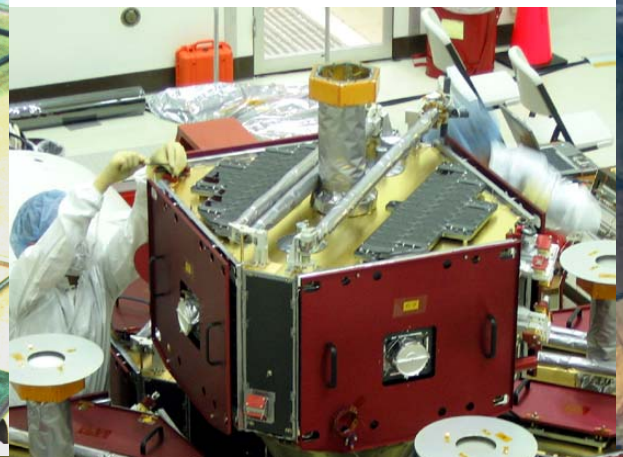

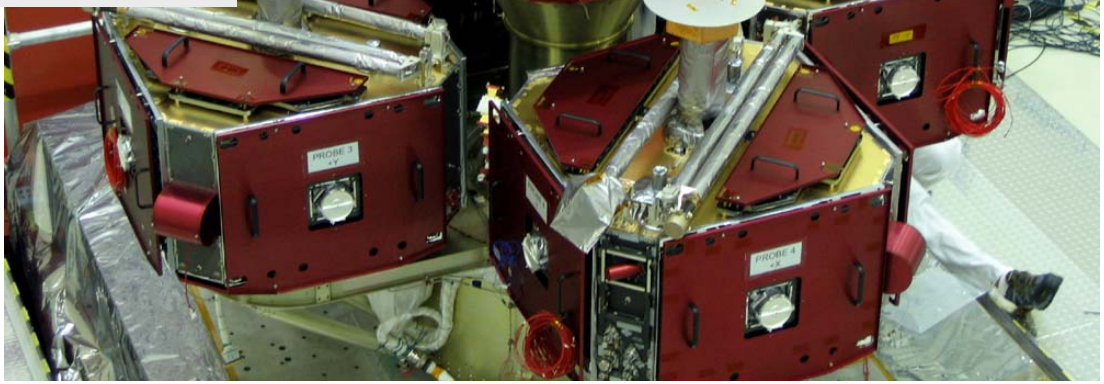

Can current plasma sensors be improved?

Of course – what hasn't been done?

High time resolution composition.

High time resolution 3-D plasma measurements.

Multi-point high resolution 3-D plasma.

Cold plasma measurements.

High energy overlap with energetic SSDs.

Elimination of background sources of noise.

THE END